

One-loop analysis of the interactions between doubly charmed baryons and Nambu-Goldstone bosons

Ze-Rui Liang,^a Peng-Cheng Qiu,^a De-Liang Yao^{a,b,1}

^a*School of Physics and Electronics, Hunan University,
410082 Changsha, China*

^b*Hunan Provincial Key Laboratory of High-Energy Scale Physics and Applications,
Hunan University, 410082 Changsha, China*

E-mail: zeruiliang@hnu.edu.cn, qiupengcheng@hnu.edu.cn,
yaodeliang@hnu.edu.cn

ABSTRACT: The interactions between the spin-1/2 doubly charmed baryons and Nambu-Goldstone bosons are analyzed within a manifestly relativistic baryon chiral perturbation theory up to next-to-next-to leading order, by using the so-called extended-on-mass-shell scheme. We utilize heavy diquark-antiquark symmetry to estimate the low-energy constants in the chiral effective Lagrangians. The S - and P -wave scattering lengths are predicted. We find that those diagrams, vanishing exactly in the heavy-quark limit, do contribute slightly to the S -wave scattering lengths in reality. The influence of the spin-3/2 doubly charmed baryons, as heavy-quark spin partners of the spin-1/2 ones, on the scattering lengths is discussed as well. Finally, S -wave phase shifts for elastic scattering processes are presented in the energy region near threshold. Our results in this work will not only be very useful for performing chiral extrapolations of future lattice QCD data, but also provide us chiral inputs for the investigation of the spectroscopy of doubly heavy baryons.

ARXIV EPRINT: [2303.03370](https://arxiv.org/abs/2303.03370)

¹Corresponding author.

Contents

1	Introduction	2
2	Formal aspects of scattering amplitude	5
2.1	Lorentz structure of the amplitude	5
2.2	Amplitudes for given strangeness and isospin	6
2.3	Partial wave projection	7
2.4	Scattering length	8
3	Calculation of the amplitude in BChPT	9
3.1	Power counting	9
3.2	Chiral effective Lagrangian	10
3.3	Tree amplitudes	11
3.4	Leading one-loop contributions	14
4	Renormalization	17
4.1	Masses and wave function renormalization constants	17
4.2	The full scattering amplitude within EOMS scheme	19
5	Numerical results and discussions	21
5.1	Parameters	21
5.2	Prediction of scattering lengths	24
5.3	Effect of spin-3/2 doubly charmed baryons	28
5.4	S -wave Phase shifts	32
6	Summary and outlook	34
A	Γ-functions and β-functions	34
B	$\tilde{\beta}$-functions	35
C	Loop corrections to the baryon masses and wave function renormalization constants	36
D	Heavy diquark-antiquark symmetry	37

1 Introduction

Over the past two decades, hadrons containing heavy quarks have been extensively explored, see e.g. Refs. [1–6] for recent reviews. This is not only because of the high experimental interest of completing the hadron spectroscopy, but also due to the theoretical importance in understanding the low-energy dynamics of quantum chromodynamics (QCD). Amongst them, the doubly heavy baryons, predicted by conventional quark model [7], have attracted quite a few attentions. They offer a unique platform for investigating the non-perturbative dynamics of light quarks in the environment of two heavy quarks and, consequently, can be used to test the correctness of theoretical frameworks such as the QCD-inspired quark model, the non-relativistic factorization theory [8] and so on.

Experimental attempts have been made to hunt for doubly heavy-flavored baryons since 2002 [9, 10], but their existence has been under controversy till 2017. In 2017, the LHCb collaboration announced the first successful observation of such states [11]. It was reported that a doubly charmed baryon Ξ_{cc}^{++} with high significance is observed via the decay mode $\Xi_{cc}^{++} \rightarrow \Lambda_c^+ K^- \pi^+ \pi^+$. The existence of the Ξ_{cc}^{++} state was later confirmed through another decay mode $\Xi_{cc}^{++} \rightarrow \Xi_c^+ \pi^+$ [12]. It should be noted that searching for doubly charmed baryons in the above two decay modes was previously suggested by the theoretical work [13]. Determinations of the properties of the Ξ_{cc}^{++} baryon are conducted subsequently, e.g., measurements of its life time [14], mass [15] and production cross section [16]. On the other hand, the quark content of Ξ_{cc}^{++} is assigned to be $[ccu]$ in the quark model. Therefore, its SU(3) partners, Ξ_{cc}^+ and Ω_{cc}^+ with contents $[ccd]$ and $[ccs]$ respectively, are expected to exist and are hoped to be observed at LHCb. Thereby, searches for the two states are carried out and are still ongoing. Yet, no evidence of observation has been found [17–19].

In fact, the search for Ξ_{cc}^+ was initially performed by the SELEX collaboration twenty years ago [9]. However, the SELEX results of Ξ_{cc}^+ reported in Refs. [9, 10] are not confirmed by any other collaborations: FOCUS at Tevatron (proton-antiproton) collider [20], BaBar and Belle at electron-positron colliders [21, 22], and LHCb at proton-proton collider [17, 18]. Even worse, the experimental value of the Ξ_{cc}^+ mass by SELEX is inconsistent with theoretical determinations obtained by relativistic quark model [23], effective potential models [24], heavy quark effective theory [25], lattice QCD [26–28], etc.. See also e.g. Ref. [29] for a brief review. The aforementioned facts lead to a long-standing puzzle in questioning the existence of doubly charmed baryons. The puzzle has been solved partly by the observation of Ξ_{cc}^{++} at LHCb [11, 12]. And hopefully, it will be addressed completely in the foreseeable future, as the LHC record condition keeps improved so as to overcome the drawbacks caused by the short life times of Ξ_{cc}^+ and Ω_{cc}^+ [30].

The discovery of the Ξ_{cc}^{++} has stimulated a multitude of works on the theoretical side. Various approaches have been employed to decipher the underlying information of these doubly heavy baryons. Static properties, decays and productions of the doubly charmed baryons have been widely studied via quark model [31–34], extended chromomagnetic model [35], SU(3) symmetry method [36, 37], operator product expansion [38], QCD sum rules [39–42], lattice QCD [43, 44] and so on.

The doubly heavy baryons are composed of two heavy quarks (Q) and one light quark

(q), where both heavy quark symmetry as $m_Q \rightarrow \infty$ and chiral symmetry as $m_q \rightarrow 0$ will manifest. Therefore, the doubly heavy baryons provide a novel platform to study heavy quark symmetry and chiral symmetry of light quarks simultaneously. In particular, the two heavy quarks in the baryons usually act as a form of compact heavy diquark. In the heavy quark limit (HQL), the heavy diquark belongs to the color $\bar{\mathbf{3}}_c$ representation and serves as a static color source for the light quarks. The same color dynamics arises in the mesons containing a single heavy antiquark. The correspondence between a heavy diquark and a single heavy antiquark is known as heavy diquark-antiquark (HDA) symmetry. In consequence, the doubly heavy baryons can be related to the mesons with a heavy antiquark component through HDA symmetry [45]. In practice, effective field theories (EFTs) are efficient and powerful in the sense that they can easily implement all such kind of symmetries through the approach of constructing pertinent effective Lagrangians.

Chiral perturbation theory (ChPT) [46–48] is the low-energy EFT of QCD, which is a powerful tool to explore hadron physics in the non-perturbative regime. It has achieved great triumphs in the pure mesonic sector. Meanwhile, various extensions have been developed in the past years [49–51]. Note that, ChPT for heavy hadrons is comprehensively reviewed in Ref. [6]. The version extended to the single-baryon sector [52] is known as baryon chiral perturbation theory (BChPT). However, when baryon fields are incorporated as explicit degrees of freedom in the theory, the notable power counting breaking (PCB) problem arises due to the non-zero mass of the baryons in the chiral limit. Many approaches have been proposed in order to remedy this issue. The most popular ones are the heavy-baryon (HB) formalism [53], the infrared regularization (IR) prescription [54] and the extended-on-mass-shell (EOMS) renormalization scheme [55]. Thereinto, the EOMS scheme not only restores the correct power counting but also respects the original analytic structure. Furthermore, it has been demonstrated that better convergence properties can be established compared to other approaches; see Refs. [50, 56] for reviews.

Within the framework of BChPT, the properties such as masses and magnetic moments of the doubly charmed baryons have been investigated in Refs. [57–64]. For the scattering of pseudoscalar Nambu-Goldstone bosons (NGB) off doubly charmed baryons, Ref. [65] conducts a lead-order (LO) BChPT calculation. Unitarization of the LO chiral amplitude is carried out so as to search for possible exotic doubly charmed states. The low-lying spectrum of the double-charm baryons with negative parity was further studied in Ref. [66] by using a chiral potential of next-to-leading order (NLO). In Ref. [67], the scattering lengths of NGB and doubly charmed baryons are calculated up to next-to-next-to-leading order (NNLO) in the HB formalism. For a relativistic chiral description of the doubly charmed baryons, complete and minimal set of chiral effective Lagrangians have already been constructed up to $O(p^4)$ in Ref. [68], with p collectively denoting the chiral expansion parameters. However, a systematical one-loop analysis of the interactions between the doubly charmed baryons and NGBs in manifestly relativistic BChPT at one-loop order is still lacking.

In present work, we have calculated the scattering amplitudes for the interactions of NGBs and doubly charmed baryons in the covariant BChPT up to NNLO, i.e. the leading one-loop order. The ultraviolet (UV) divergences stemming from the loops are removed

by utilizing the modified minimal subtraction scheme, namely, the $\overline{\text{MS}} - 1$ scheme. Furthermore, we have explicitly checked that the PCB terms can be absorbed exactly via a finite shifts of the low energy constants (LECs) according to the essence of EOMS scheme. In this way, we obtain the EOMS-renormalized chiral amplitude, which is renormalization-scale independent and can be used to derive physical observable of interest. Moreover, the obtained one-loop amplitudes possess proper analytic structure and correct power counting. And hence they are very suited to perform chiral extrapolation, when relevant lattice QCD data are available in future. In addition, our one-loop amplitudes can be applied to evaluate finite-volume corrections of lattice QCD results by merely substituting all the involved one-loop integrals with their finite counterparts that are uniformly formulated in Ref. [69].

For the lack of available data from experiments or lattice QCD at present, we have to estimate the unknown LECs in chiral effective Lagrangians by imposing the HDA symmetry mentioned above. Specifically, the unknown LECs in our case can be related to the ones involved in the $D\phi$ scatterings, where D and ϕ stand for charmed D mesons and NGBs, respectively. Fortunately, the values $D\phi$ LECs have been well determined by performing fits to lattice QCD data of the S -wave $D\phi$ scattering lengths in Refs. [70–73]. In fact, two of the $\mathcal{O}(p^2)$ LECs, b_1 and b_2 , have been determined by fitting to lattice QCD data on the doubly charmed baryon masses in Ref. [63]. We find that the values of b_1 and b_2 obtained in Ref. [63] agree well with those by HDA symmetry, indicating the feasibility of the use of HDA symmetry in this work. The remaining LECs, that can not be constrained by HDA symmetry, are set to zero in line with the ansatz of naturalness of LECs.

Given that the LECs are pinned down, we predict the S - and P -wave scattering lengths for the elastic channels with definite strangeness S and isospin I . For S -wave scattering lengths, our relativistic results turn out to be qualitatively consistent with the ones obtained in the HB approach [67]. Sizable relativistic recoil corrections exist, for instance, in the channel of $\Xi_{cc}\bar{K} \rightarrow \Xi_{cc}\bar{K}$ with $(S, I) = (-1, 0)$. In Ref. [67], the contributions from the diagrams, which should vanish exactly only in the HQL, are ignored. We have explicitly verified that those HQL-vanishing diagrams indeed contribute marginally to the S -wave scattering lengths in the real world with a finite heavy quark mass. In HQL, since the spin-3/2 and spin-1/2 doubly charmed baryons degenerate into a heavy quark spin (HQS) multiplet, they should be treated on equal footing. Therefore, we assess the influence of the spin-3/2 states on the scattering lengths by incorporating them as explicit degrees of freedom into the effective Lagrangians. As expected, they mainly affect the P -wave scattering lengths with quantum numbers $J^P = \frac{3}{2}^+$. Their contributions to the S -wave scattering lengths are negligible. As byproducts, we also discuss the so-called resonance contribution to the LECs by integrating out the spin-3/2 baryons.

For future reference, S -wave phase shifts are calculated for the channels of elastic scatterings in the energy regions close to the lowest thresholds under consideration. Future lattice QCD simulations of the low-energy interactions between doubly charmed baryons and NGBs are necessary to explore the spectrum of the doubly heavy baryons. Our S -wave phase shifts can be associated directly with the energy levels at non-zero momenta via the famous Lüscher formula [74] and its generalizations [75–78].

The layout of this manuscript is described as follows. Formal aspects for the scattering

amplitude are introduced in section 2, where Lorentz decomposition, the strangeness-isospin structure and partial wave projection are briefly illustrated. Details on the calculation of the chiral amplitudes are exhibited in section 3. Chiral effective lagrangians relevant to our calculation up to NNLO are displayed in subsection 3.2. Tree-level and loop amplitudes are given in subsections 3.3 and 3.4, respectively. Section 4 complies the procedure of renormalization of the one-loop amplitudes within the EOMS scheme. In section 5.1, the values of the LECs are estimated. The S -wave and P -wave scattering lengths are calculated in subsection 5.2. Subsection 5.3 discusses the impact of the spin-3/2 doubly charmed baryons. The S -wave phase shifts for the channels of elastic scatterings are presented in subsection 5.4. Finally, section 6 comprises our summary and outlook. The β -functions concerning the UV- and EOMS-subtractions are relegated to appendices A and B, respectively. Appendix C contains the definition of loop integrals and explicit expressions of loop corrections for the masses and wave function renormalization constants. Application of HDA symmetry to the estimation of the LEC values is detailed in appendix D.

2 Formal aspects of scattering amplitude

2.1 Lorentz structure of the amplitude

The scattering process of $\psi_1(p)\phi_1(q) \rightarrow \psi_2(p')\phi_2(q')$, with momenta indicated in parentheses, is described by the Lorentz-invariant amplitude, which can be decomposed as

$$\mathcal{T}_{\psi_1\phi_1 \rightarrow \psi_2\phi_2}(s, t) = \bar{u}(p', \sigma') \left\{ A(s, t) + \frac{1}{2}(\not{q} + \not{q}')B(s, t) \right\} u(p, \sigma). \quad (2.1)$$

Here, $\psi_{1,2} \in \{\Xi_{cc}^{++}, \Xi_{cc}^+, \Omega_{cc}^+\}$ represent the incoming and outgoing doubly charmed baryons respectively, while $\phi_{1,2} \in \{\pi^\pm, \pi^0, K^\pm, K^0, \bar{K}^0, \eta\}$ are the incoming and outgoing Goldstone bosons in order. The symbols σ and σ' denote the spins of the corresponding baryons. The Mandelstam variables are defined by

$$s = (p + q)^2, \quad t = (p - p')^2, \quad u = (p - q')^2, \quad (2.2)$$

which satisfy the constraint $s + t + u = m_{\psi_1}^2 + m_{\phi_1}^2 + m_{\psi_2}^2 + m_{\phi_2}^2 \equiv \Sigma$. The Lorentz decomposition of the scattering amplitude is not unique, an alternative form is given by

$$\mathcal{T}_{\psi_1\phi_1 \rightarrow \psi_2\phi_2}(s, t) = \bar{u}(p', \sigma') \left\{ D(s, t) + \frac{i\sigma^{\mu\nu} q'_\mu q_\nu}{m_{\psi_1} + m_{\psi_2}} B(s, t) \right\} u(p, \sigma), \quad (2.3)$$

with $\sigma^{\mu\nu} = \frac{i}{2}[\gamma^\mu, \gamma^\nu]$. The new function $D(s, t)$ is related to A and B via

$$D(s, t) = A(s, t) + \nu B(s, t), \quad \nu = \frac{s - u}{2(m_{\psi_1} + m_{\psi_2})}. \quad (2.4)$$

Similar to the situation in pion-nucleon scattering, the decomposition in terms of D and B is more suited to perform chiral expansion [79], while the other is more practically convenient for the extraction of the structure functions A and B .

2.2 Amplitudes for given strangeness and isospin

The doubly charmed baryons and the pseudoscalar NGBs fill the representations of the SU(3) flavor group of the light (u, d, s) quarks. Namely, they belong to the SU(3) triplets and octets, respectively. In consequence, there exist a multitude of physical scattering amplitudes corresponding to the various charge states showing up in the multiplets. These scattering amplitudes can be classified, thanks to the conservation of strangeness (S) and isospin (I). As a result, the general meson-baryon scattering processes can be categorized into 7 independent channels of interactions: 4 single-channel processes and 3 coupled-channel ones. In practice, the amplitudes with definite (S, I) quantum numbers can be expressed in terms of the physical amplitudes. Explicit relations are listed in the following.

(i) For the single channels with $(S, I) = (-2, \frac{1}{2}), (1, 1), (1, 0), (0, \frac{3}{2})$, one has

$$\mathcal{T}_{\Omega_{cc}\bar{K}\rightarrow\Omega_{cc}\bar{K}}^{(-2, \frac{1}{2})}(s, t, u) = \mathcal{T}_{\Omega_{cc}^+K^-\rightarrow\Omega_{cc}^+K^-}(s, t, u), \quad (2.5)$$

$$\mathcal{T}_{\Xi_{cc}K\rightarrow\Xi_{cc}K}^{(1, 1)}(s, t, u) = \mathcal{T}_{\Xi_{cc}^{++}K^+\rightarrow\Xi_{cc}^{++}K^+}(s, t, u), \quad (2.6)$$

$$\mathcal{T}_{\Xi_{cc}K\rightarrow\Xi_{cc}K}^{(1, 0)}(s, t, u) = 2\mathcal{T}_{\Xi_{cc}^{++}K^0\rightarrow\Xi_{cc}^{++}K^0}(s, t, u) - \mathcal{T}_{\Xi_{cc}^{++}K^+\rightarrow\Xi_{cc}^{++}K^+}(s, t, u), \quad (2.7)$$

$$\mathcal{T}_{\Xi_{cc}\pi\rightarrow\Xi_{cc}\pi}^{(0, \frac{3}{2})}(s, t, u) = \mathcal{T}_{\Xi_{cc}^{++}\pi^+\rightarrow\Xi_{cc}^{++}\pi^+}(s, t, u). \quad (2.8)$$

(ii) For the two-coupled channel with $(S, I) = (-1, 1)$, the relations are given by

$$\mathcal{T}_{\Omega_{cc}\pi\rightarrow\Omega_{cc}\pi}^{(-1, 1)}(s, t, u) = \mathcal{T}_{\Omega_{cc}^+\pi^0\rightarrow\Omega_{cc}^+\pi^0}(s, t, u), \quad (2.9)$$

$$\mathcal{T}_{\Xi_{cc}\bar{K}\rightarrow\Xi_{cc}\bar{K}}^{(-1, 1)}(s, t, u) = \mathcal{T}_{\Xi_{cc}^{++}K^0\rightarrow\Xi_{cc}^{++}K^0}(u, t, s), \quad (2.10)$$

$$\mathcal{T}_{\Omega_{cc}\pi\rightarrow\Xi_{cc}\bar{K}}^{(-1, 1)}(s, t, u) = \sqrt{2}\mathcal{T}_{\Xi_{cc}^{++}K^-\rightarrow\Omega_{cc}^+\pi^0}(s, t, u). \quad (2.11)$$

(iii) For the two-coupled channel with $(S, I) = (-1, 0)$, the relations can be written as

$$\mathcal{T}_{\Xi_{cc}\bar{K}\rightarrow\Xi_{cc}\bar{K}}^{(-1, 0)}(s, t, u) = 2\mathcal{T}_{\Xi_{cc}^{++}K^+\rightarrow\Xi_{cc}^{++}K^+}(u, t, s) - \mathcal{T}_{\Xi_{cc}^{++}K^0\rightarrow\Xi_{cc}^{++}K^0}(u, t, s), \quad (2.12)$$

$$\mathcal{T}_{\Omega_{cc}\eta\rightarrow\Omega_{cc}\eta}^{(-1, 0)}(s, t, u) = \mathcal{T}_{\Omega_{cc}^+\eta\rightarrow\Omega_{cc}^+\eta}(s, t, u), \quad (2.13)$$

$$\mathcal{T}_{\Xi_{cc}\bar{K}\rightarrow\Omega_{cc}\eta}^{(-1, 0)}(s, t, u) = \sqrt{2}\mathcal{T}_{\Xi_{cc}^+\bar{K}^0\rightarrow\Omega_{cc}^+\eta}(s, t, u). \quad (2.14)$$

(iv) For the three-coupled channel with $(S, I) = (0, \frac{1}{2})$, the relations read

$$\mathcal{T}_{\Xi_{cc}\pi\rightarrow\Xi_{cc}\pi}^{(0, \frac{1}{2})}(s, t, u) = \frac{3}{2}\mathcal{T}_{\Xi_{cc}^{++}\pi^+\rightarrow\Xi_{cc}^{++}\pi^+}(u, t, s) - \frac{1}{2}\mathcal{T}_{\Xi_{cc}^{++}\pi^+\rightarrow\Xi_{cc}^{++}\pi^+}(s, t, u), \quad (2.15)$$

$$\mathcal{T}_{\Xi_{cc}\eta\rightarrow\Xi_{cc}\eta}^{(0, \frac{1}{2})}(s, t, u) = \mathcal{T}_{\Xi_{cc}^{++}\eta\rightarrow\Xi_{cc}^{++}\eta}(s, t, u), \quad (2.16)$$

$$\mathcal{T}_{\Omega_{cc}K\rightarrow\Omega_{cc}K}^{(0, \frac{1}{2})}(s, t, u) = \mathcal{T}_{\Omega_{cc}^+K^-\rightarrow\Omega_{cc}^+K^-}(u, t, s), \quad (2.17)$$

$$\mathcal{T}_{\Xi_{cc}\pi\rightarrow\Xi_{cc}\pi}^{(0, \frac{1}{2})}(s, t, u) = \sqrt{3}\mathcal{T}_{\Xi_{cc}^{++}\pi^0\rightarrow\Xi_{cc}^{++}\pi^0}(s, t, u), \quad (2.18)$$

$$\mathcal{T}_{\Xi_{cc}\pi\rightarrow\Omega_{cc}K}^{(0, \frac{1}{2})}(s, t, u) = \sqrt{3}\mathcal{T}_{\Xi_{cc}^{++}K^-\rightarrow\Omega_{cc}^+\pi^0}(u, t, s), \quad (2.19)$$

$$\mathcal{T}_{\Xi_{cc}\eta\rightarrow\Omega_{cc}K}^{(0, \frac{1}{2})}(s, t, u) = \mathcal{T}_{\Xi_{cc}^+\bar{K}^0\rightarrow\Omega_{cc}^+\eta}(u, t, s). \quad (2.20)$$

In above, there are in total 16 scattering amplitudes with definite strangeness and isospin. Nevertheless, they can be expressed in terms of 10 physical amplitudes, provided that crossing symmetry is implemented.

2.3 Partial wave projection

The partial wave expansion of the scattering amplitude takes the form [80, 81]

$$\begin{aligned} \mathcal{T}_{\psi_1\phi_1\rightarrow\psi_2\phi_2}^{(S,I)}(s, t) = & \sqrt{2m_{\psi_1}}\sqrt{2m_{\psi_2}}\chi_{\psi_2}^\dagger \sum_{\ell=0}^{\infty} \left\{ [(\ell+1)\mathcal{T}_{\ell+}^{(S,I)}(s) + \ell\mathcal{T}_{\ell-}^{(S,I)}(s)]P_\ell(z) \right. \\ & \left. - [\mathcal{T}_{\ell+}^{(S,I)}(s) - \mathcal{T}_{\ell-}^{(S,I)}(s)]i\boldsymbol{\sigma} \cdot (\hat{\mathbf{q}}' \times \hat{\mathbf{q}}) P'_\ell(z) \right\} \chi_{\psi_1}, \end{aligned} \quad (2.21)$$

where $\boldsymbol{\sigma} = (\sigma_1, \sigma_2, \sigma_3)$ is a vector with components being Pauli matrices, and χ (χ^\dagger) is the spinor of the incoming (outgoing) baryon. Furthermore, $\hat{\mathbf{q}} = \mathbf{q}/|\mathbf{q}|$ and $\hat{\mathbf{q}}' = \mathbf{q}'/|\mathbf{q}'|$ are the directions of the incoming and outgoing Goldstone mesons, respectively. $P_\ell(z)$ is the Legendre polynomial and $P'_\ell(z)$ is its derivative. $z = \cos\theta$ with θ the scattering angle. Here ℓ is the orbital momentum, and the notation $\ell\pm$ indicates the total angular momentum is $J = \ell \pm \frac{1}{2}$.

In Eq. (2.21), the amplitude $\mathcal{T}_{\ell\pm}^{(S,I)}$ is the so-called dimensionless partial-wave amplitude, which possesses definite quantum numbers of strangeness S , isospin I and total angular momentum J . It is popular to redefine a new partial wave amplitude $f_{\ell\pm}^{(S,I)}$ via

$$\mathcal{T}_{\ell\pm}^{(S,I)}(s) = \frac{8\pi\sqrt{s}}{\sqrt{2m_{\psi_1}}\sqrt{2m_{\psi_2}}} f_{\ell\pm}^{(S,I)}(s), \quad (2.22)$$

which is more preferable in investigations of the analytic properties [82]. The inversion of Eq. (2.21) yields

$$\begin{aligned} f_{\ell\pm}^{(S,I)}(s) = & \frac{\sqrt{E_{\psi_1} + m_{\psi_1}}\sqrt{E_{\psi_2} + m_{\psi_2}}}{16\pi\sqrt{s}} \left\{ A_\ell^{(S,I)}(s) + \frac{E_{\phi_1} + E_{\phi_2}}{2} B_\ell^{(S,I)}(s) + \left[\frac{|\mathbf{q}|^2}{2(E_{\psi_1} + m_{\psi_1})} \right. \right. \\ & \left. \left. + \frac{|\mathbf{q}'|^2}{2(E_{\psi_2} + m_{\psi_2})} \right] B_\ell^{(S,I)}(s) + |\mathbf{q}||\mathbf{q}'| \left[\frac{B_{\ell\pm 1}^{(S,I)}(s)}{2(E_{\psi_1} + m_{\psi_1})} + \frac{B_{\ell\pm 1}^{(S,I)}(s)}{2(E_{\psi_2} + m_{\psi_2})} \right. \right. \\ & \left. \left. - \frac{A_{\ell\pm 1}^{(S,I)}(s) - \frac{E_{\phi_1} + E_{\phi_2}}{2} B_{\ell\pm 1}^{(S,I)}(s)}{(E_{\psi_1} + m_{\psi_1})(E_{\psi_2} + m_{\psi_2})} \right] \right\}, \end{aligned} \quad (2.23)$$

where $A_\ell^{(S,I)}$ and $B_\ell^{(S,I)}$ are given by

$$\begin{aligned} A_\ell^{(S,I)}(s) &= \int_{-1}^1 d\cos\theta P_\ell(\cos\theta) A^{(S,I)}(s, t) \Big|_{t=m_{\psi_1}^2 + m_{\psi_2}^2 - 2E_{\psi_1}E_{\psi_2} + 2|\mathbf{q}||\mathbf{q}'|\cos\theta}, \\ B_\ell^{(S,I)}(s) &= \int_{-1}^1 d\cos\theta P_\ell(\cos\theta) B^{(S,I)}(s, t) \Big|_{t=m_{\psi_1}^2 + m_{\psi_2}^2 - 2E_{\psi_1}E_{\psi_2} + 2|\mathbf{q}||\mathbf{q}'|\cos\theta}. \end{aligned} \quad (2.24)$$

In the above equations, E_{ψ_1} (E_{ψ_2}) is the energy of the incoming (outgoing) doubly charmed baryon, E_{ϕ_1} (E_{ϕ_2}) denotes the energy of the incoming (outgoing) meson, and \mathbf{q} (\mathbf{q}') stands

for the three momentum of the incoming (outgoing) meson. In the center-of-mass (CM) frame, one has

$$E_{\psi_i} = \frac{s + m_{\psi_i}^2 - m_{\phi_i}^2}{2\sqrt{s}}, \quad E_{\phi_i} = \frac{s - m_{\psi_i}^2 + m_{\phi_i}^2}{2\sqrt{s}}, \quad (i = 1, 2)$$

$$|\mathbf{q}|^2 = \frac{1}{4s} \lambda(s, m_{\psi_1}^2, m_{\phi_1}^2), \quad |\mathbf{q}'|^2 = \frac{1}{4s} \lambda(s, m_{\psi_2}^2, m_{\phi_2}^2), \quad (2.25)$$

with $\lambda(a, b, c) = a^2 + b^2 + c^2 - 2ab - 2ac - 2bc$ being the Källén function.

For an elastic scattering process $\psi\phi \rightarrow \psi\phi$, the relevant partial wave amplitude $f_{\ell\pm}^{(S,I)}(s)$ in Eq. (2.23) can be simplified to [83, 84]

$$f_{\ell\pm}^{(S,I)}(s) = \frac{1}{16\pi\sqrt{s}} \left\{ (E + m_\psi) \left[A_\ell^{(S,I)}(s) + (\sqrt{s} - m_\psi) B_\ell^{(S,I)}(s) \right] \right. \\ \left. + (E - m_\psi) \left[-A_{\ell\pm 1}^{(S,I)}(s) + (\sqrt{s} + m_\psi) B_{\ell\pm 1}^{(S,I)}(s) \right] \right\}, \quad (2.26)$$

with

$$A_\ell^{(S,I)}(s) = \int_{-1}^1 d\cos\theta P_\ell(\cos\theta) A^{(S,I)}(s, t) |_{t=-2\mathbf{q}^2(1-\cos\theta)},$$

$$B_\ell^{(S,I)}(s) = \int_{-1}^1 d\cos\theta P_\ell(\cos\theta) B^{(S,I)}(s, t) |_{t=-2\mathbf{q}^2(1-\cos\theta)}. \quad (2.27)$$

Here $E = (s + m_\psi^2 - m_\phi^2)/(2\sqrt{s})$ is the CM energy of doubly charmed baryon and $|\mathbf{q}| = \lambda^{1/2}(s, m_\psi^2, m_\phi^2)/(2\sqrt{s})$ refers to the modulus of the CM momentum.

2.4 Scattering length

Scattering length is one of the most important quantities characterizing the properties of strong interaction. In what follows, we derive the formulae for the calculation of the scattering lengths in the elastic scattering channels.

In the vicinity of threshold, the amplitudes $f_{\ell\pm}^{(S,I)}(s)$ in Eq. (2.26) can be expanded in terms of the three momentum squared \mathbf{q}^2 ,

$$f_{\ell\pm}^{(S,I)}(s) = a_{\ell\pm}^{(S,I)} \mathbf{q}^{2\ell} + b_{\ell\pm}^{(S,I)} \mathbf{q}^{2\ell+2} + c_{\ell\pm}^{(S,I)} \mathbf{q}^{2\ell+4} + \mathcal{O}(\mathbf{q}^{2\ell+6}). \quad (2.28)$$

The coefficients on the right hand side of the above equation are referred to as threshold parameters. Specifically, the coefficients of the first three terms, $a_{\ell\pm}^{(S,I)}$, $b_{\ell\pm}^{(S,I)}$ and $c_{\ell\pm}^{(S,I)}$, are called scattering lengths¹, effective ranges and shape parameters, in order.

In view of Eq. (2.26), the threshold expansion of $f_{\ell\pm}^{(S,I)}(s)$ can be obtained by expanding $A_\ell^{(S,I)}(s)$ and $B_\ell^{(S,I)}(s)$ in the same way as Eq. (2.28), i.e.,

$$A_\ell^{(S,I)}(s) = A_\ell^{(S,I,\ell)} \mathbf{q}^{2\ell} + A_\ell^{(S,I,\ell+1)} \mathbf{q}^{2\ell+2} + A_\ell^{(S,I,\ell+2)} \mathbf{q}^{2\ell+4} + \mathcal{O}(\mathbf{q}^{2\ell+6}),$$

$$B_\ell^{(S,I)}(s) = B_\ell^{(S,I,\ell)} \mathbf{q}^{2\ell} + B_\ell^{(S,I,\ell+1)} \mathbf{q}^{2\ell+2} + B_\ell^{(S,I,\ell+2)} \mathbf{q}^{2\ell+4} + \mathcal{O}(\mathbf{q}^{2\ell+6}). \quad (2.29)$$

¹The scattering lengths for the P waves are also called scattering volumes.

Therefore, the S - and P -wave scattering lengths of our interest can be written as

$$\begin{aligned}
a_{0+}^{(S,I)} &= \frac{m_\psi}{8\pi(m_\psi + m_\phi)} \left(A_0^{(S,I,0)} + m_\phi B_0^{(S,I,0)} \right), \\
a_{1+}^{(S,I)} &= \frac{m_\psi}{8\pi(m_\psi + m_\phi)} \left(A_1^{(S,I,1)} + m_\phi B_1^{(S,I,1)} \right), \\
a_{1-}^{(S,I)} &= a_{1+}^{(S,I)} + \frac{1}{32\pi m_\psi(m_\psi + m_\phi)} \left(-A_0^{(S,I,0)} + (2m_\psi + m_\phi) B_0^{(S,I,0)} \right). \quad (2.30)
\end{aligned}$$

On the other hand, for small t , $A^{(S,I)}(s, t)$ and $B^{(S,I)}(s, t)$ can be expressed as

$$\begin{aligned}
A^{(S,I)}(s, t) &= A^{(S,I)}(s, 0) + t \left[\partial_t A^{(S,I)}(s, t) \right]_{t=0} + \frac{t^2}{2} \left[\partial_t^2 A^{(S,I)}(s, t) \right]_{t=0} + \dots, \\
B^{(S,I)}(s, t) &= B^{(S,I)}(s, 0) + t \left[\partial_t B^{(S,I)}(s, t) \right]_{t=0} + \frac{t^2}{2} \left[\partial_t^2 B^{(S,I)}(s, t) \right]_{t=0} + \dots. \quad (2.31)
\end{aligned}$$

Substituting Eq. (2.31) in to Eq. (2.27), one can obtain the coefficients in Eq. (2.29). For S and P waves, we get

$$\begin{aligned}
A_0^{(S,I,0)} &= 2 \left[A^{(S,I)}(s, 0) \right]_{\mathbf{q}^2=0}, \quad B_0^{(S,I,0)} = 2 \left[B^{(S,I)}(s, 0) \right]_{\mathbf{q}^2=0}, \\
A_1^{(S,I,1)} &= \frac{4}{3} \left[\partial_t A^{(S,I)}(s, t) \right]_{t=0, \mathbf{q}^2=0}, \quad B_1^{(S,I,1)} = \frac{4}{3} \left[\partial_t B^{(S,I)}(s, t) \right]_{t=0, \mathbf{q}^2=0}. \quad (2.32)
\end{aligned}$$

Eventually, with the help of Eq. (2.32) and Eq. (2.30), the S - and P -wave scattering lengths in terms of A and B amplitudes are expressed as²

$$\begin{aligned}
a_{0+}^{(S,I)} &= \frac{m_\psi}{4\pi(m_\psi + m_\phi)} \left\{ \left[A^{(S,I)}(s, 0) \right]_{\mathbf{q}^2=0} + m_\phi \left[B^{(S,I)}(s, 0) \right]_{\mathbf{q}^2=0} \right\}, \\
a_{1+}^{(S,I)} &= \frac{m_\psi}{6\pi(m_\psi + m_\phi)} \left\{ \left[\partial_t A^{(S,I)}(s, t) \right]_{t=0, \mathbf{q}^2=0} + m_\phi \left[\partial_t B^{(S,I)}(s, t) \right]_{t=0, \mathbf{q}^2=0} \right\}, \\
a_{1-}^{(S,I)} &= a_{1+}^{(S,I)} - \frac{1}{16\pi m_\psi(m_\psi + m_\phi)} \left\{ \left[A^{(S,I)}(s, 0) \right]_{\mathbf{q}^2=0} - (2m_\psi + m_\phi) \left[B^{(S,I)}(s, 0) \right]_{\mathbf{q}^2=0} \right\}. \quad (2.33)
\end{aligned}$$

Given that the expressions of the A and B functions are known, the above formulae can be readily applied to obtain the scattering lengths analytically.

3 Calculation of the amplitude in BChPT

3.1 Power counting

The amplitudes for the processes of on-shell scatterings are multivariate functions of masses and Mandelstam variables. Since the baryon masses are non-zero in the chiral limit, the chiral expansion of the amplitudes in the vicinity of threshold can be organized in powers of the following quantities,

$$\frac{s - m_{\psi_1/\psi_2}^2}{\Lambda_\chi^2} \sim \frac{u - m_{\psi_1/\psi_2}^2}{\Lambda_\chi^2} \sim \frac{m_{\phi_1/\phi_2}}{\Lambda_\chi} \ll 1, \quad \frac{t}{\Lambda_\chi^2} \ll 1, \quad (3.1)$$

²Our notation of the S -wave scattering length is the same as the one used in Ref. [67], but different from the definition in Ref. [65] by a factor of 1/2, i.e., $a_{0+} = a_{0+}^{\text{Guo}}/2$.

with Λ_χ denoting the chiral symmetry breaking scale. Accordingly, the power counting rules for those parameters are set as

$$\begin{aligned} m_{\psi_1/\psi_2} &\sim \mathcal{O}(p^0), & m_{\phi_1/\phi_2} &\sim \mathcal{O}(p^1), & s - m_{\psi_1/\psi_2}^2 &\sim \mathcal{O}(p^1), \\ u - m_{\psi_1/\psi_2}^2 &\sim \mathcal{O}(p^1), & t &\sim \mathcal{O}(p^2), \end{aligned} \quad (3.2)$$

where p is a collective symbol representing the small parameters.

An important feature in BChPT is that each Feynman diagram under consideration is characterized by a chiral dimension D . Namely, the importance of the diagram is regarded to be the order of $(p/\Lambda_\chi)^D$. In our case of one-baryon sector, the chiral dimension D for a given diagram can be determined by the naive power counting rule,

$$D = 4L + \sum_n nV_n - 2I_\phi - I_\psi, \quad (3.3)$$

with L the number of loops, V_n the number of the n^{th} -order vertices, I_ϕ the number of internal pion lines, and I_ψ the number of internal doubly charmed baryon lines.

However, there exist pieces in the loop amplitudes, originating from the diagrams with internal baryon lines, which violates the above power counting rule (3.3). These pieces are known as PCB terms, as mentioned in the Introduction. The emergence of PCB terms is due to the fact that the masses of doubly charmed baryons do not vanish in the chiral limit, as pointed out by Ref. [52]. We will address this issue by using the EOMS scheme in section 4.

3.2 Chiral effective Lagrangian

The chiral effective Lagrangian, which is relevant to our calculation of the meson-baryon scattering amplitude up to $\mathcal{O}(p^3)$, takes the form

$$\mathcal{L}_{\text{eff}} = \sum_{i=1}^2 \mathcal{L}_{\phi\phi}^{(2i)} + \sum_{j=1}^3 \mathcal{L}_{\psi\phi}^{(j)}, \quad (3.4)$$

with the superscripts ‘ $2i$ ’ and ‘ j ’ in the brackets representing the chiral dimensions. For the purely mesonic sector, we need the following terms [48]

$$\mathcal{L}_{\phi\phi}^{(2)} = \frac{F^2}{4} \langle \partial_\mu U \partial^\mu U^\dagger \rangle + \frac{F^2}{4} \langle \chi U^\dagger + U \chi^\dagger \rangle, \quad (3.5)$$

$$\begin{aligned} \mathcal{L}_{\phi\phi}^{(4)} &= L_4 \langle \partial_\mu U \partial^\mu U^\dagger \rangle \langle \chi U^\dagger + U \chi^\dagger \rangle + L_5 \langle \partial_\mu U \partial^\mu U^\dagger (\chi U^\dagger + U \chi^\dagger) \rangle + L_6 \langle \chi U^\dagger + U \chi^\dagger \rangle^2 \\ &+ L_8 \langle U \chi^\dagger U \chi^\dagger + \chi U^\dagger \chi U^\dagger \rangle + \dots, \end{aligned} \quad (3.6)$$

where $\langle \dots \rangle$ stands for the trace in the flavor space, F is the pion decay constant in the SU(3) chiral limit [51, 85], and L_k ($k = 4, 5, 6, 8$) denote the mesonic LECs. The NGB fields are collected in U , which reads

$$U = \exp\left(i\sqrt{2}\phi/F\right), \quad \phi = \begin{pmatrix} \frac{1}{\sqrt{2}}\pi^0 + \frac{1}{\sqrt{6}}\eta & \pi^+ & K^+ \\ \pi^- & -\frac{1}{\sqrt{2}}\pi^0 + \frac{1}{\sqrt{6}}\eta & K^0 \\ K^- & \bar{K}^0 & -\frac{2}{\sqrt{6}}\eta \end{pmatrix}. \quad (3.7)$$

Furthermore, in the isospin limit $m_u = m_d = \hat{m}$, the chiral operator χ can be written as

$$\chi = 2B_0 s = \text{diag} (m_\pi^2, m_\pi^2, 2m_K^2 - m_\pi^2), \quad (3.8)$$

where $B_0 = -\langle 0|\bar{q}q|0\rangle/3F^2$, and $\langle 0|\bar{q}q|0\rangle$ is the quark condensate in the chiral limit [47].

For the baryonic sector, we proceed with the SU(3) triplet ψ in which the doubly charmed baryons are contained. The physical states Ξ_{cc}^{++} , Ξ_{cc}^+ and Ω_{cc}^+ form the baryon triplet ψ , which reads

$$\psi = \begin{pmatrix} \Xi_{cc}^{++} \\ \Xi_{cc}^+ \\ \Omega_{cc}^+ \end{pmatrix}. \quad (3.9)$$

The full set of the chiral operators up to and including $\mathcal{O}(p^4)$, describing the interactions between Goldstone bosons and doubly charmed baryons, is constructed in Ref. [68]. In our current case, the required terms are given as follows:

$$\mathcal{L}_{\psi\phi}^{(1)} = \bar{\psi} (i\not{D} - m) \psi + \frac{g}{2} \bar{\psi} \not{\psi} \gamma_5 \psi, \quad (3.10)$$

$$\begin{aligned} \mathcal{L}_{\psi\phi}^{(2)} = & b_1 \bar{\psi} \langle \chi_+ \rangle \psi + b_2 \bar{\psi} \tilde{\chi}_+ \psi + b_3 \bar{\psi} u^2 \psi + b_4 \bar{\psi} \langle u^2 \rangle \psi + \frac{b_5}{m^2} \bar{\psi} (\{u^\mu, u^\nu\} D_{\mu\nu} + H.c.) \psi \\ & + \frac{b_6}{m^2} \bar{\psi} (\langle u^\mu u^\nu \rangle D_{\mu\nu} + H.c.) \psi + ib_7 \bar{\psi} [u^\mu, u^\nu] \sigma_{\mu\nu} \psi, \end{aligned} \quad (3.11)$$

$$\begin{aligned} \mathcal{L}_{\psi\phi}^{(3)} = & ic_{11} \bar{\psi} [u_\mu, h^{\mu\nu}] \gamma_\nu \psi + \frac{c_{12}}{m^2} \bar{\psi} (i [u^\mu, h^{\nu\rho}] \gamma_\mu D_{\nu\rho} + H.c.) \psi + \frac{c_{13}}{m} \bar{\psi} (i \{u^\mu, h^{\nu\rho}\} \sigma_{\mu\nu} D_\rho \\ & + H.c.) \psi + \frac{c_{14}}{m} \bar{\psi} (i \sigma_{\mu\nu} \langle u^\mu h^{\nu\rho} \rangle D_\rho + H.c.) \psi + c_{15} \bar{\psi} \{u^\mu, \tilde{\chi}_+\} \gamma_5 \gamma_\mu \psi \\ & + c_{16} \bar{\psi} u^\mu \gamma_5 \gamma_\mu \langle \chi_+ \rangle \psi + c_{17} \bar{\psi} \gamma_5 \gamma_\mu \langle u^\mu \tilde{\chi}_+ \rangle \psi + ic_{18} \bar{\psi} \gamma_5 \gamma_\mu [D^\mu, \tilde{\chi}_-] \psi \\ & + ic_{19} \bar{\psi} \gamma_5 \gamma_\mu \langle [D^\mu, \chi_-] \rangle \psi + c_{20} \bar{\psi} [\tilde{\chi}_-, u^\mu] \gamma_\mu \psi, \end{aligned} \quad (3.12)$$

where

$$\begin{aligned} D_\mu &= \partial_\mu + \Gamma_\mu, & \Gamma_\mu &= \frac{1}{2} [u^\dagger \partial_\mu u + u \partial_\mu u^\dagger], \\ u_\mu &= i [u^\dagger \partial_\mu u - u \partial_\mu u^\dagger], & u &= U^{\frac{1}{2}}, \\ \chi_\pm &= u^\dagger \chi u^\dagger \pm u \chi^\dagger u, & \tilde{\chi}_\pm &= \chi_\pm - \frac{1}{3} \langle \chi_\pm \rangle, \\ h_{\mu\nu} &= D_\mu u_\nu + D_\nu u_\mu, & D_{\mu\nu} &= \{D_\mu, D_\nu\}. \end{aligned} \quad (3.13)$$

Here, m is the baryon mass in the chiral limit and g denotes the bare axial-vector coupling constant. The baryonic LECs b_j ($j = 1, \dots, 7$) and c_k ($k = 11, \dots, 20$) are unknown parameters in units of GeV^{-1} and GeV^{-2} , respectively. *H.c.* stands for terms obtained by hermitian conjugation.

3.3 Tree amplitudes

According to the aforementioned power counting rule, the tree-level Feynman diagrams contributing to the meson-baryon scattering amplitude up to $\mathcal{O}(p^3)$ are shown in Figure 1. Note that the corresponding crossed diagrams are not displayed in Figure 1.

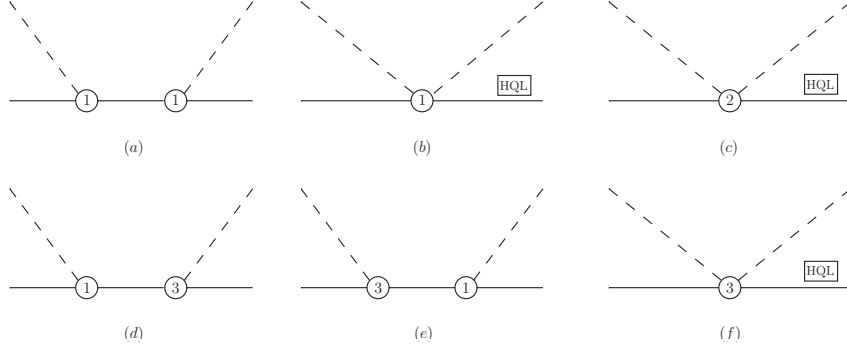


Figure 1. Tree diagrams for $\psi\phi$ scattering up to $\mathcal{O}(p^3)$. The solid and dashed lines stand for doubly charmed baryons and NGBs, respectively. The relevant crossed diagrams are not shown explicitly. Diagrams surviving in the HQL are indicated by boxed “HQL”.

The LO tree-level amplitude takes the following form

$$\begin{aligned} A_{\text{tree}}^{(1)} &= \frac{g^2}{8F^2} \left[\mathcal{C}_S^{(1)} \mathcal{F}(s) + \mathcal{C}_U^{(1)} \mathcal{F}(u) \right] , \\ B_{\text{tree}}^{(1)} &= \frac{\mathcal{C}_{\text{WT}}^{(1)}}{4F^2} - \frac{g^2}{4F^2} \left[\mathcal{C}_S^{(1)} \mathcal{G}(s) - \mathcal{C}_U^{(1)} \mathcal{G}(u) \right] , \end{aligned} \quad (3.14)$$

with the functions \mathcal{F} and \mathcal{G} defined by

$$\begin{aligned} \mathcal{F}(s) &= \frac{(m_{\psi_1} + m_{\psi_2})(s - m_{\psi_1} m_{\psi_2}) + m(2s - m_{\psi_1}^2 - m_{\psi_2}^2)}{s - m^2} , \\ \mathcal{G}(s) &= \frac{s + m_{\psi_1} m_{\psi_2} + m(m_{\psi_1} + m_{\psi_2})}{s - m^2} , \end{aligned} \quad (3.15)$$

where m is the mass of the intermediate doubly charmed baryons in the chiral limit. All the involved coefficients are given in Table 1. The Weinberg-Tomazawa (WT) term, accompanied by the coefficient $\mathcal{C}_{\text{WT}}^{(1)}$, stems from diagram (b) in Figure 1. The s -channel diagram (a) gives the terms proportional to $\mathcal{C}_S^{(1)}$, while its crossed partner yields the pieces with coefficient $\mathcal{C}_U^{(1)}$.

The $\mathcal{O}(p^2)$ meson-baryon scattering amplitude reads

$$\begin{aligned} A_{\text{tree}}^{(2)} &= \frac{\mathcal{C}_1^{(2)}}{6F^2} + \mathcal{C}_2^{(2)} \frac{m_{\phi_1}^2 + m_{\phi_2}^2 - t}{2F^2} + \frac{\mathcal{C}_3^{(2)}}{2m^2 F^2} \mathcal{H}(s, t) + \mathcal{C}_4^{(2)} \frac{u - s}{F^2} , \\ B_{\text{tree}}^{(2)} &= \mathcal{C}_4^{(2)} \frac{2(m_{\psi_1} + m_{\psi_2})}{F^2} , \end{aligned} \quad (3.16)$$

with

$$\mathcal{H}(s, t) = 2su - (s + u)\Sigma + m_{\psi_1}^4 + m_{\psi_2}^4 + 2m_{\phi_1}^2 m_{\phi_2}^2 + (m_{\psi_1}^2 + m_{\psi_2}^2)(m_{\phi_1}^2 + m_{\phi_2}^2) . \quad (3.17)$$

The coefficients $\mathcal{C}_i^{(2)}$ ($i = 1, \dots, 4$) are compiled in Table 2. All of these coefficients are obtained from diagram (c) of Figure 1.

Table 1. Coefficients appearing in the tree amplitudes of $\mathcal{O}(p^1)$. The exchanged doubly charmed baryons are indicated in the square brackets. The scattering processes are categorized by strangeness S and isospin I .

(S, I)	Processes	$\mathcal{C}_{\text{WT}}^{(1)}$	$\mathcal{C}_S^{(1)}$	$\mathcal{C}_U^{(1)}$
$(-2, \frac{1}{2})$	$\Omega_{cc}\bar{K} \rightarrow \Omega_{cc}\bar{K}$	-2	0	2 [Ξ_{cc}]
$(1, 1)$	$\Xi_{cc}K \rightarrow \Xi_{cc}K$	-2	0	2 [Ω_{cc}]
$(1, 0)$	$\Xi_{cc}K \rightarrow \Xi_{cc}K$	2	0	-2 [Ω_{cc}]
$(0, \frac{3}{2})$	$\Xi_{cc}\pi \rightarrow \Xi_{cc}\pi$	-2	0	2 [Ξ_{cc}]
$(-1, 0)$	$\Xi_{cc}\bar{K} \rightarrow \Xi_{cc}\bar{K}$	4	4 [Ω_{cc}]	0
	$\Omega_{cc}\eta \rightarrow \Omega_{cc}\eta$	0	$\frac{4}{3}$ [Ω_{cc}]	$\frac{4}{3}$ [Ω_{cc}]
	$\Xi_{cc}\bar{K} \rightarrow \Omega_{cc}\eta$	$-2\sqrt{3}$	$-\frac{4}{\sqrt{3}}$ [Ω_{cc}]	$\frac{2}{\sqrt{3}}$ [Ξ_{cc}]
$(-1, 1)$	$\Omega_{cc}\pi \rightarrow \Omega_{cc}\pi$	0	0	0
	$\Xi_{cc}\bar{K} \rightarrow \Xi_{cc}\bar{K}$	0	0	0
	$\Omega_{cc}\pi \rightarrow \Xi_{cc}\bar{K}$	-2	0	2 [Ξ_{cc}]
$(0, \frac{1}{2})$	$\Xi_{cc}\pi \rightarrow \Xi_{cc}\pi$	4	3 [Ξ_{cc}]	-1 [Ξ_{cc}]
	$\Xi_{cc}\eta \rightarrow \Xi_{cc}\eta$	0	$\frac{1}{3}$ [Ξ_{cc}]	$\frac{1}{3}$ [Ξ_{cc}]
	$\Omega_{cc}K \rightarrow \Omega_{cc}K$	2	2 [Ξ_{cc}]	0
	$\Xi_{cc}\pi \rightarrow \Xi_{cc}\eta$	0	1 [Ξ_{cc}]	1 [Ξ_{cc}]
	$\Xi_{cc}\pi \rightarrow \Omega_{cc}K$	$\sqrt{6}$	$\sqrt{6}$ [Ξ_{cc}]	0
	$\Xi_{cc}\eta \rightarrow \Omega_{cc}K$	$\sqrt{6}$	$\frac{\sqrt{6}}{3}$ [Ξ_{cc}]	$-\frac{2\sqrt{6}}{3}$ [Ω_{cc}]

Table 2. Coefficients in the tree amplitudes of $\mathcal{O}(p^2)$.

(S, I)	Processes	$\mathcal{C}_1^{(2)}$	$\mathcal{C}_2^{(2)}$	$\mathcal{C}_3^{(2)}$	$\mathcal{C}_4^{(2)}$
$(-2, \frac{1}{2})$	$\Omega_{cc}\bar{K} \rightarrow \Omega_{cc}\bar{K}$	$-4(6b_1 + b_2)m_K^2$	$2(b_3 + 2b_4)$	$4(b_5 + b_6)$	$-2b_7$
$(1, 1)$	$\Xi_{cc}K \rightarrow \Xi_{cc}K$	$-4(6b_1 + b_2)m_K^2$	$2(b_3 + 2b_4)$	$4(b_5 + b_6)$	$-2b_7$
$(1, 0)$	$\Xi_{cc}K \rightarrow \Xi_{cc}K$	$-4(6b_1 - 5b_2)m_K^2$	$-2(b_3 - 2b_4)$	$-4(b_5 - b_6)$	$2b_7$
$(0, \frac{3}{2})$	$\Xi_{cc}\pi \rightarrow \Xi_{cc}\pi$	$-4(6b_1 + b_2)m_\pi^2$	$2(b_3 + 2b_4)$	$4(b_5 + b_6)$	$-2b_7$
$(-1, 0)$	$\Xi_{cc}\bar{K} \rightarrow \Xi_{cc}\bar{K}$	$-8(3b_1 + 2b_2)m_K^2$	$4(b_3 + b_4)$	$4(2b_5 + b_6)$	$4b_7$
	$\Omega_{cc}\eta \rightarrow \Omega_{cc}\eta$	$-\frac{32}{3}(3b_1 + 2b_2)m_K^2 + (8b_1 + \frac{40}{3}b_2)m_\pi^2$	$\frac{4}{3}(2b_3 + 3b_4)$	$\frac{4}{3}(4b_5 + 3b_6)$	0
	$\Xi_{cc}\bar{K} \rightarrow \Omega_{cc}\eta$	$2\sqrt{3}b_2(5m_K^2 - 3m_\pi^2)$	$-\frac{2}{\sqrt{3}}b_3$	$-\frac{4}{\sqrt{3}}b_5$	$-2\sqrt{3}b_7$
$(-1, 1)$	$\Omega_{cc}\pi \rightarrow \Omega_{cc}\pi$	$-8(3b_1 - b_2)m_\pi^2$	$4b_4$	$4b_6$	0
	$\Xi_{cc}\bar{K} \rightarrow \Xi_{cc}\bar{K}$	$-8(3b_1 - b_2)m_K^2$	$4b_4$	$4b_6$	0
	$\Omega_{cc}\pi \rightarrow \Xi_{cc}\bar{K}$	$-6b_2(m_K^2 + m_\pi^2)$	$2b_3$	$4b_5$	$-2b_7$
$(0, \frac{1}{2})$	$\Xi_{cc}\pi \rightarrow \Xi_{cc}\pi$	$-4(6b_1 + b_2)m_\pi^2$	$2(b_3 + 2b_4)$	$4(b_5 + b_6)$	$4b_7$
	$\Xi_{cc}\eta \rightarrow \Xi_{cc}\eta$	$-\frac{32}{3}(3b_1 - b_2)m_K^2 + (8b_1 - \frac{20}{3}b_2)m_\pi^2$	$\frac{2}{3}(b_3 + 6b_4)$	$\frac{4}{3}(b_5 + 3b_6)$	0
	$\Omega_{cc}K \rightarrow \Omega_{cc}K$	$-4(6b_1 + b_2)m_K^2$	$2(b_3 + 2b_4)$	$4(b_5 + b_6)$	$2b_7$
	$\Xi_{cc}\pi \rightarrow \Xi_{cc}\eta$	$-12b_2m_\pi^2$	$2b_3$	$4b_5$	0
	$\Xi_{cc}\pi \rightarrow \Omega_{cc}K$	$-3\sqrt{6}b_2(m_K^2 + m_\pi^2)$	$\sqrt{6}b_3$	$2\sqrt{6}b_5$	$\sqrt{6}b_7$
	$\Xi_{cc}\eta \rightarrow \Omega_{cc}K$	$\sqrt{6}b_2(5m_K^2 - 3m_\pi^2)$	$-\frac{\sqrt{6}}{3}b_3$	$-\frac{2\sqrt{6}}{3}b_5$	$\sqrt{6}b_7$

The tree-level amplitude at $\mathcal{O}(p^3)$ can be written as

$$\begin{aligned}
A_{\text{tree}}^{(3)} &= \mathcal{C}_2^{(3)} \frac{(m_{\psi_2} - m_{\psi_1})}{m^2 F^2} \left[(m_{\phi_1}^2 - m_{\phi_2}^2)t + (m_{\psi_2}^2 - m_{\psi_1}^2)(s - u) \right] \\
&+ \mathcal{C}_3^{(3)} \frac{(s - u)^2}{m F^2} + (\mathcal{C}_4^{(3)} + \mathcal{C}_5^{(3)}) \frac{m_{\psi_2} - m_{\psi_1}}{2 F^2} \\
&+ \frac{g}{4 F^2} \left[(\mathcal{C}_6^{(3)} + \mathcal{C}_8^{(3)}) \mathcal{F}(s) + (\mathcal{C}_7^{(3)} + \mathcal{C}_9^{(3)}) \mathcal{F}(u) \right], \\
B_{\text{tree}}^{(3)} &= \mathcal{C}_1^{(3)} \frac{2(m_{\phi_1}^2 + m_{\phi_2}^2 - t)}{F^2} - \frac{2\mathcal{C}_2^{(3)}}{m^2 F^2} \left[\mathcal{H}(s, t) + (s - u)^2 + (m_{\phi_1}^2 - m_{\phi_2}^2)^2 \right] \\
&- \mathcal{C}_3^{(3)} \frac{2(s - u)(m_{\psi_1} + m_{\psi_2})}{m F^2} - \frac{2(\mathcal{C}_4^{(3)} - \mathcal{C}_5^{(3)})}{F^2} \\
&- \frac{g}{2 F^2} \left[(\mathcal{C}_6^{(3)} + \mathcal{C}_8^{(3)}) \mathcal{G}(s) - (\mathcal{C}_7^{(3)} + \mathcal{C}_9^{(3)}) \mathcal{G}(u) \right]. \tag{3.18}
\end{aligned}$$

The coefficients are shown in Tables 3, 4 and 5. The $\mathcal{C}_i^{(3)}$ ($i = 1, \dots, 5$) are obtained from diagram (f), which corresponds to the contact contribution of $\mathcal{O}(p^3)$. The s -channel exchange diagrams, (d) and (e), generate the terms with coefficients $\mathcal{C}_6^{(3)}$ and $\mathcal{C}_8^{(3)}$, and their crossed diagrams are responsible for the contributions with coefficients $\mathcal{C}_7^{(3)}$ and $\mathcal{C}_9^{(3)}$.

Table 3. Coefficients in the tree amplitudes of $\mathcal{O}(p^3)$.

(S, I)	Processes	$\mathcal{C}_1^{(3)}$	$\mathcal{C}_2^{(3)}$	$\mathcal{C}_3^{(3)}$	$\mathcal{C}_4^{(3)}$	$\mathcal{C}_5^{(3)}$
$(-2, \frac{1}{2})$	$\Omega_{cc}\bar{K} \rightarrow \Omega_{cc}\bar{K}$	$-2c_{11}$	$-2c_{12}$	$2(c_{13} + c_{14})$	$2c_{20}m_K^2$	$-2c_{20}m_K^2$
$(1, 1)$	$\Xi_{cc}K \rightarrow \Xi_{cc}K$	$-2c_{11}$	$-2c_{12}$	$2(c_{13} + c_{14})$	$2c_{20}m_K^2$	$-2c_{20}m_K^2$
$(1, 0)$	$\Xi_{cc}K \rightarrow \Xi_{cc}K$	$2c_{11}$	$2c_{12}$	$-2(c_{13} - c_{14})$	$-2c_{20}m_K^2$	$2c_{20}m_K^2$
$(0, \frac{3}{2})$	$\Xi_{cc}\pi \rightarrow \Xi_{cc}\pi$	$-2c_{11}$	$-2c_{12}$	$2(c_{13} + c_{14})$	$2c_{20}m_\pi^2$	$-2c_{20}m_\pi^2$
$(-1, 0)$	$\Xi_{cc}\bar{K} \rightarrow \Xi_{cc}\bar{K}$	$4c_{11}$	$4c_{12}$	$2(2c_{13} + c_{14})$	$-4c_{20}m_K^2$	$4c_{20}m_K^2$
	$\Omega_{cc}\eta \rightarrow \Omega_{cc}\eta$	0	0	$\frac{2}{3}(4c_{13} + 3c_{14})$	0	0
	$\Xi_{cc}\bar{K} \rightarrow \Omega_{cc}\eta$	$-2\sqrt{3}c_{11}$	$-2\sqrt{3}c_{12}$	$-\frac{2\sqrt{3}}{3}c_{13}$	$\frac{1}{\sqrt{3}}c_{20}(5m_K^2 + m_\pi^2)$	$-\sqrt{3}c_{20}(3m_K^2 - m_\pi^2)$
$(-1, 1)$	$\Omega_{cc}\pi \rightarrow \Omega_{cc}\pi$	0	0	$2c_{14}$	0	0
	$\Xi_{cc}\bar{K} \rightarrow \Xi_{cc}\bar{K}$	0	0	$2c_{14}$	0	0
	$\Omega_{cc}\pi \rightarrow \Xi_{cc}\bar{K}$	$-2c_{11}$	$-2c_{12}$	$2c_{13}$	$-c_{20}(m_K^2 - 3m_\pi^2)$	$-c_{20}(3m_K^2 - m_\pi^2)$
$(0, \frac{1}{2})$	$\Xi_{cc}\pi \rightarrow \Xi_{cc}\pi$	$4c_{11}$	$4c_{12}$	$2(c_{13} + c_{14})$	$-4c_{20}m_\pi^2$	$4c_{20}m_\pi^2$
	$\Xi_{cc}\eta \rightarrow \Xi_{cc}\eta$	0	0	$\frac{2}{3}c_{13} + 2c_{14}$	0	0
	$\Omega_{cc}K \rightarrow \Omega_{cc}K$	$2c_{11}$	$2c_{12}$	$2(c_{13} + c_{14})$	$-2c_{20}m_K^2$	$2c_{20}m_K^2$
	$\Xi_{cc}\pi \rightarrow \Xi_{cc}\eta$	0	0	$2c_{13}$	0	0
	$\Xi_{cc}\pi \rightarrow \Omega_{cc}K$	$\sqrt{6}c_{11}$	$\sqrt{6}c_{12}$	$\sqrt{6}c_{13}$	$\frac{\sqrt{6}}{2}c_{20}(m_K^2 - 3m_\pi^2)$	$\frac{\sqrt{6}}{2}c_{20}(3m_K^2 - m_\pi^2)$
	$\Xi_{cc}\eta \rightarrow \Omega_{cc}K$	$\sqrt{6}c_{11}$	$\sqrt{6}c_{12}$	$-\frac{\sqrt{6}}{3}c_{13}$	$-\frac{\sqrt{6}}{2}c_{20}(3m_K^2 - m_\pi^2)$	$\frac{1}{\sqrt{6}}c_{20}(5m_K^2 + m_\pi^2)$

3.4 Leading one-loop contributions

One-loop Feynman diagrams relevant to our calculation at $\mathcal{O}(p^3)$ are exhibited in Figure 2. Crossed diagrams are not shown. There are 34 loop diagrams in total. We have calculated all of them. Explicit analytical expressions for the 16 processes have been obtained. However, the expressions are too lengthy to be displayed here.³ For the loop

³Explicit expressions of all the one-loop amplitudes are obtainable from the authors.

Table 4. Coefficients in the tree amplitudes of $\mathcal{O}(p^3)$. The exchanged doubly charmed baryons are indicated in the square brackets. The combination $\mathcal{C}_{8-6}^{(3)} = \mathcal{C}_8^{(3)} - \mathcal{C}_6^{(3)}$ is used for brevity.

(S, I)	Processes	$\mathcal{C}_6^{(3)}$	$\mathcal{C}_{8-6}^{(3)}$
$(-2, \frac{1}{2})$	$\Omega_{cc}\bar{K} \rightarrow \Omega_{cc}\bar{K}$	0	0
$(1, 1)$	$\Xi_{cc}K \rightarrow \Xi_{cc}K$	0	0
$(1, 0)$	$\Xi_{cc}K \rightarrow \Xi_{cc}K$	0	0
$(0, \frac{3}{2})$	$\Xi_{cc}\pi \rightarrow \Xi_{cc}\pi$	0	0
$(-1, 0)$	$\Xi_{cc}\bar{K} \rightarrow \Xi_{cc}\bar{K}$	$-\frac{8}{3}(2c_{15} + 6c_{16} - 3c_{18})m_K^2 + (\frac{16}{3}c_{15} - 8c_{16})m_\pi^2$	$[\Omega_{cc}]$
	$\Omega_{cc}\eta \rightarrow \Omega_{cc}\eta$	$\frac{8}{9}(8c_{15} - 3c_{16} + 6c_{17} - c_{18} - 6c_{19})m_\pi^2 - \frac{16}{9}(4c_{15} + 3c_{16} + 3c_{17} - 2c_{18} - 3c_{19})m_K^2$	$[\Omega_{cc}]$
	$\Xi_{cc}\bar{K} \rightarrow \Omega_{cc}\eta$	$\frac{8\sqrt{3}}{9}((2c_{15} + 6c_{16} - 3c_{18})m_K^2 - (2c_{15} - 3c_{16})m_\pi^2)$	$[\Omega_{cc}]$
$(-1, 1)$	$\Omega_{cc}\pi \rightarrow \Omega_{cc}\pi$	0	0
	$\Xi_{cc}\bar{K} \rightarrow \Xi_{cc}\bar{K}$	0	0
	$\Omega_{cc}\pi \rightarrow \Xi_{cc}\bar{K}$	0	0
$(0, \frac{1}{2})$	$\Xi_{cc}\pi \rightarrow \Xi_{cc}\pi$	$4(2c_{15} - 3c_{16})m_K^2 - 2(4c_{15} + 3c_{16} - 3c_{18})m_\pi^2$	$[\Xi_{cc}]$
	$\Xi_{cc}\eta \rightarrow \Xi_{cc}\eta$	$\frac{4}{9}(2c_{15} - 3c_{16} + 6c_{17} + 2c_{18} - 6c_{19})m_K^2 - \frac{2}{9}(4c_{15} + 3c_{16} + 12c_{17} + c_{18} - 12c_{19})m_\pi^2$	$[\Xi_{cc}]$
	$\Omega_{cc}K \rightarrow \Omega_{cc}K$	$(-\frac{8}{3}c_{15} - 8c_{16} + 4c_{18})m_K^2 + (\frac{8}{3}c_{15} - 4c_{16})m_\pi^2$	$[\Xi_{cc}]$
	$\Xi_{cc}\pi \rightarrow \Xi_{cc}\eta$	$(\frac{8}{3}c_{15} - 4c_{16})m_K^2 - (\frac{8}{3}c_{15} + 2c_{16} - 2c_{18})m_\pi^2$	$[\Xi_{cc}]$
	$\Xi_{cc}\pi \rightarrow \Omega_{cc}K$	$\frac{4\sqrt{6}}{3}(2c_{15} - 3c_{16})m_K^2 - \frac{2\sqrt{6}}{3}(4c_{15} + 3c_{16} - 3c_{18})m_\pi^2$	$[\Xi_{cc}]$
	$\Xi_{cc}\eta \rightarrow \Omega_{cc}K$	$\frac{4\sqrt{6}}{9}(2c_{15} - 3c_{16} + 6c_{17} + 2c_{18} - 6c_{19})m_K^2 - \frac{2\sqrt{6}}{9}(4c_{15} + 3c_{16} + 12c_{17} + c_{18} - 12c_{19})m_\pi^2$	$[\Xi_{cc}]$
		$\Delta_1 = \frac{8}{3\sqrt{3}}(6c_{15} + 6c_{17} - c_{18} - 6c_{19})(m_K^2 - m_\pi^2)$	
		$\Delta_2 = \frac{8}{3}(3c_{17} + c_{18} - 3c_{19})(m_K^2 - m_\pi^2)$	
		$\Delta_3 = -2\sqrt{6}(2c_{15} - c_{18})(m_K^2 - m_\pi^2)$	
		$\Delta_4 = -\frac{2\sqrt{6}}{9}(6c_{15} + 12c_{17} + c_{18} - 12c_{19})(m_K^2 - m_\pi^2)$	

Abbreviations:

Table 5. Coefficients in the tree amplitudes of $\mathcal{O}(p^3)$. The exchanged doubly charmed baryons are indicated in the square brackets. The combination $\mathcal{C}_{9-7}^{(3)} = \mathcal{C}_9^{(3)} - \mathcal{C}_7^{(3)}$ is used for brevity.

(S, I)	Processes	$\mathcal{C}_7^{(3)}$	$\mathcal{C}_{9-7}^{(3)}$
$(-2, \frac{1}{2})$	$\Omega_{cc}\bar{K} \rightarrow \Omega_{cc}\bar{K}$	$(-\frac{8}{3}c_{15} - 8c_{16} + 4c_{18})m_K^2 + (\frac{8}{3}c_{15} - 4c_{16})m_\pi^2$	$[\Xi_{cc}]$
$(1, 1)$	$\Xi_{cc}K \rightarrow \Xi_{cc}K$	$(-\frac{8}{3}c_{15} - 8c_{16} + 4c_{18})m_K^2 + (\frac{8}{3}c_{15} - 4c_{16})m_\pi^2$	$[\Omega_{cc}]$
$(1, 0)$	$\Xi_{cc}K \rightarrow \Xi_{cc}K$	$(\frac{8}{3}c_{15} + 8c_{16} - 4c_{18})m_K^2 - (\frac{8}{3}c_{15} - 4c_{16})m_\pi^2$	$[\Omega_{cc}]$
$(0, \frac{3}{2})$	$\Xi_{cc}\pi \rightarrow \Xi_{cc}\pi$	$(\frac{16}{3}c_{15} - 8c_{16})m_K^2 - (\frac{16}{3}c_{15} + 4c_{16} - 4c_{18})m_\pi^2$	$[\Xi_{cc}]$
$(-1, 0)$	$\Xi_{cc}\bar{K} \rightarrow \Xi_{cc}\bar{K}$	0	0
	$\Omega_{cc}\eta \rightarrow \Omega_{cc}\eta$	$-\frac{16}{9}(4c_{15} + 3c_{17} - 2c_{18} - 3c_{19})m_K^2 + \frac{8}{9}(8c_{15} - 3c_{16} + 6c_{17} - c_{18} - 6c_{19})m_\pi^2$	$[\Omega_{cc}]$
	$\Xi_{cc}\bar{K} \rightarrow \Omega_{cc}\eta$	$\frac{4}{3\sqrt{3}}(2(2c_{15} - 3c_{16} + 6c_{17} + 2c_{18} - 6c_{19})m_K^2 - (4c_{15} + 3c_{16} + 12c_{17} + c_{18} - 12c_{19})m_\pi^2)$	$[\Xi_{cc}]$
$(-1, 1)$	$\Omega_{cc}\pi \rightarrow \Omega_{cc}\pi$	0	0
	$\Xi_{cc}\bar{K} \rightarrow \Xi_{cc}\bar{K}$	0	0
	$\Omega_{cc}\pi \rightarrow \Xi_{cc}\bar{K}$	$(-\frac{8}{3}c_{15} - 8c_{16} + 4c_{18})m_K^2 + (\frac{8}{3}c_{15} - 4c_{16})m_\pi^2$	$[\Xi_{cc}]$
$(0, \frac{1}{2})$	$\Xi_{cc}\pi \rightarrow \Xi_{cc}\pi$	$(-\frac{8}{3}c_{15} + 4c_{16})m_K^2 + (\frac{8}{3}c_{15} + 2c_{16} - 2c_{18})m_\pi^2$	$[\Xi_{cc}]$
	$\Xi_{cc}\eta \rightarrow \Xi_{cc}\eta$	$\frac{4}{9}(2c_{15} - 3c_{16} + 6c_{17} + 2c_{18} - 6c_{19})m_K^2 - \frac{2}{9}(4c_{15} + 3c_{16} + 12c_{17} + c_{18} - 12c_{19})m_\pi^2$	$[\Xi_{cc}]$
	$\Omega_{cc}K \rightarrow \Omega_{cc}K$	0	0
	$\Xi_{cc}\pi \rightarrow \Xi_{cc}\eta$	$\frac{4}{3}(2c_{15} - 3c_{16} + 6c_{17} + 2c_{18} - 6c_{19})m_K^2 - \frac{2}{3}(4c_{15} + 3c_{16} + 12c_{17} + c_{18} - 12c_{19})m_\pi^2$	$[\Xi_{cc}]$
	$\Xi_{cc}\pi \rightarrow \Omega_{cc}K$	0	0
	$\Xi_{cc}\eta \rightarrow \Omega_{cc}K$	$\frac{4\sqrt{6}}{9}((2c_{15} + 6c_{16} - 3c_{18})m_K^2 - (2c_{15} - 3c_{16})m_\pi^2)$	$[\Omega_{cc}]$
Abbreviations:			
		$\Delta'_1 = -\frac{4}{3\sqrt{3}}(6c_{15} + 12c_{17} + c_{18} - 12c_{19})(m_K^2 - m_\pi^2)$	
		$\Delta'_2 = 4(2c_{15} - c_{18})(m_K^2 - m_\pi^2)$	
		$\Delta'_3 = -\frac{8}{3}(3c_{17} + c_{18} - 3c_{19})(m_K^2 - m_\pi^2)$	
		$\Delta'_4 = \frac{4\sqrt{6}}{9}(6c_{15} + 6c_{17} - c_{18} - 6c_{19})(m_K^2 - m_\pi^2)$	

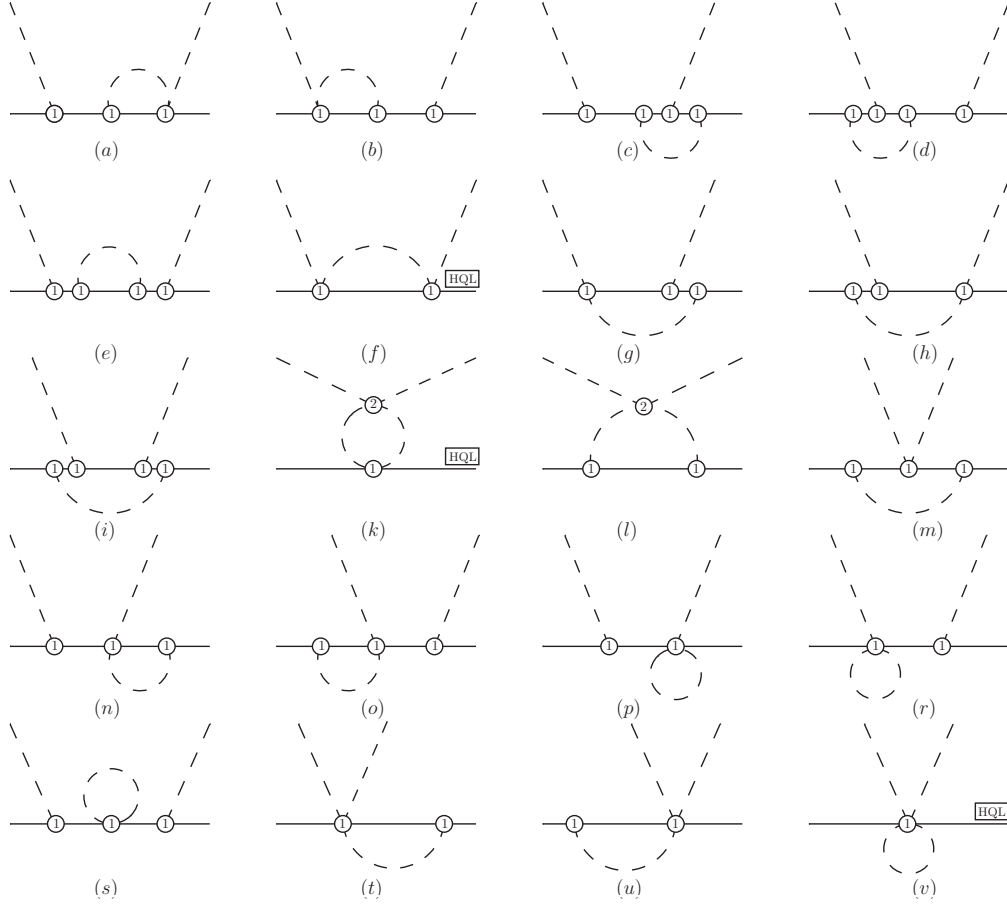


Figure 2. One-loop Feynman diagrams contributing to $\psi\phi$ scattering at $\mathcal{O}(p^3)$. Crossed diagrams are not shown. In addition, diagrams with loop corrections on external legs are taken into account via wave function renormalization. Diagrams surviving in the HQL are indicated by boxed “HQL”.

amplitudes, we do not need to distinguish the physical masses and the bare masses, since the caused difference is of higher order beyond our accuracy. Note that the contributions of diagrams corresponding to one-loop corrections on the external legs are incorporated via wave function renormalization, which will be discussed in the next section.

4 Renormalization

4.1 Masses and wave function renormalization constants

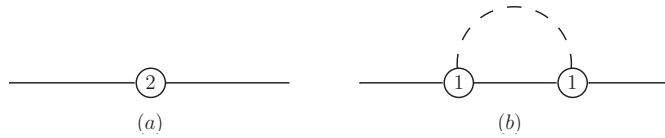


Figure 3. Tree and one-loop self-energy diagrams up to $\mathcal{O}(p^3)$.

Let us begin with the baryonic sector. The dressed propagator of the doubly charmed baryons is defined as

$$iS_\psi(p) = \frac{i}{\not{p} - m - \Sigma_\psi(\not{p})}, \quad \psi \in \{\Xi_{cc}^{++}, \Xi_{cc}^+, \Omega_{cc}^+\}, \quad (4.1)$$

where m denotes the bare baryon mass and $\Sigma_\psi(\not{p})$ refers to the baryon self-energy up to leading one-loop order. The sum of one-particle-irreducible diagrams contributing to the two-point function is denoted by $-i\Sigma_\psi(\not{p})$, which comprises contact and one-loop diagrams shown in Figure 3. Namely, one has

$$-i\Sigma_\psi(\not{p}) = -i\zeta_\psi^\dagger [\Sigma_a(\not{p}) + \Sigma_b(\not{p})] \zeta_\psi, \quad (4.2)$$

where ζ_ψ are unit vectors in the SU(3) flavor spaces,

$$\zeta_{\Xi_{cc}^{++}} = \begin{pmatrix} 1 \\ 0 \\ 0 \end{pmatrix}, \quad \zeta_{\Xi_{cc}^+} = \begin{pmatrix} 0 \\ 1 \\ 0 \end{pmatrix}, \quad \zeta_{\Omega_{cc}^+} = \begin{pmatrix} 0 \\ 0 \\ 1 \end{pmatrix}. \quad (4.3)$$

Furthermore, the chiral results for the self energies in Eq. (4.2) are given by

$$\begin{aligned} \Sigma_a^{ij}(\not{p}) &= -2[(b_1 - \frac{1}{3}b_2)\langle\chi\rangle\delta^{ij} + b_2\chi^{ij}], \\ \Sigma_b^{ij}(\not{p}) &= \frac{g^2}{8F^2s}\lambda_c^{ik}\lambda_c^{kj} \left\{ 2s m_{\psi_k} [A_0(m_{\psi_k}^2) + m_{\phi_c}^2 B_0(s, m_{\psi_k}^2, m_{\phi_c}^2)] \right. \\ &\quad + \not{p} [(s - m_{\psi_k}^2)A_0(m_{\phi_c}^2) + (s + m_{\psi_k}^2)A_0(m_{\psi_k}^2) \\ &\quad \left. + [s(m_{\phi_c}^2 - s) + m_{\psi_k}^2(2s + m_{\phi_c}^2) - m_{\psi_k}^4]B_0(s, m_{\psi_k}^2, m_{\phi_c}^2)] \right\}, \quad (4.4) \end{aligned}$$

with $i, j, k \in \{1, 2, 3\}$ and $c \in \{1, \dots, 8\}$. The definition of loop integrals A_0 and B_0 can be found in Appendix C. The NGB mass matrix χ is defined in Eq. (3.8) and λ 's are the standard Gell-mann matrices. Summation over repeated indices is implied. In addition, the masses of the intermediate states, showing up in the loop, are specified according to

$$m_{\psi_k} = \begin{cases} m_{\Xi_{cc}}, & k = 1, 2 \\ m_{\Omega_{cc}}, & k = 3 \end{cases}, \quad m_{\phi_c} = \begin{cases} m_\pi, & c = 1, 2, 3 \\ m_K, & c = 4, \dots, 7 \\ m_\eta, & c = 8 \end{cases}. \quad (4.5)$$

The pole position of the dressed propagator (4.1) defines the physical mass m_ψ of the baryon. That is,

$$[\not{p} - m + \Sigma_\psi(\not{p})]_{\not{p}=m_\psi} = 0. \quad (4.6)$$

With the help of Eq. (4.2) and Eq. (4.4), the physical masses of the doubly charmed baryons can be expressed as

$$m_{\Xi_{cc}} = m + \frac{4}{3}b_2(m_K^2 - m_\pi^2) - 2b_1(2m_K^2 + m_\pi^2) + \delta m_{\Xi_{cc}}^{\text{loop}}, \quad (4.7)$$

$$m_{\Omega_{cc}} = m - \frac{8}{3}b_2(m_K^2 - m_\pi^2) - 2b_1(2m_K^2 + m_\pi^2) + \delta m_{\Omega_{cc}}^{\text{loop}}, \quad (4.8)$$

where $\delta m_{\Xi_{cc}}^{\text{loop}}$ and $\delta m_{\Omega_{cc}}^{\text{loop}}$ are given in Eq. (C.5).

The wave function renormalization constant is defined as the residue of the pole term of the dressed propagator,

$$iS_\psi = \frac{i\mathcal{Z}_\psi}{\not{p} - m_\psi} + \text{non-pole pieces}, \quad (4.9)$$

where m_ψ is the physical baryon mass as specified in Eq. (4.6). In view of Eq. (4.1), the wave function renormalization constant \mathcal{Z}_ψ is given by

$$\mathcal{Z}_\psi = \frac{1}{1 - \Sigma'_\psi(m_\psi)} \simeq 1 + \Sigma'_\psi(m_\psi), \quad (4.10)$$

where a prime means performing derivative with respect to \not{p} . Explicit expression of \mathcal{Z}_ψ can be readily obtained by substituting Eq. (4.4) into the above equation. The readers are referred to Appendix C for the final results for $\mathcal{Z}_{\Xi_{cc}}$ and $\mathcal{Z}_{\Omega_{cc}}$.

Likewise, one can derive the wave function renormalization constants for the Goldstone bosons. Nevertheless, they have been extensively calculated elsewhere [48, 51, 86]. For completeness, we quote the results in the following

$$\mathcal{Z}_\pi = 1 - \frac{1}{3F^2} \left\{ 24 [2L_4 m_K^2 + (L_4 + L_5) m_\pi^2] + A_0(m_K^2) + 2A_0(m_\pi^2) \right\}, \quad (4.11)$$

$$\mathcal{Z}_K = 1 - \frac{1}{4F^2} \left\{ 32 [(2L_4 + L_5) m_K^2 + L_4 m_\pi^2] + A_0(m_\eta^2) + 2A_0(m_K^2) + A_0(m_\pi^2) \right\}, \quad (4.12)$$

$$\mathcal{Z}_\eta = 1 + \frac{1}{3F^2} \left\{ 8 [(L_5 - 3L_4) m_\pi^2 - (4L_5 + 6L_4) m_K^2] - 3A_0(m_K^2) \right\}. \quad (4.13)$$

4.2 The full scattering amplitude within EOMS scheme

The Lehmann-Symanzik-Zimmermann (LSZ) reduction formula indicates that the full scattering amplitude, i.e. the on-shell transition amplitude, is related to the amputated Green function $\widehat{\mathcal{T}}$ in the momentum space through

$$\mathcal{T}_{\psi_1\phi_1 \rightarrow \psi_2\phi_2}(s, t) = \mathcal{Z}_{\psi_1}^{\frac{1}{2}} \mathcal{Z}_{\phi_1}^{\frac{1}{2}} \mathcal{Z}_{\psi_2}^{\frac{1}{2}} \mathcal{Z}_{\phi_2}^{\frac{1}{2}} \bar{u}(p', \sigma') \widehat{\mathcal{T}}_{\psi_1\phi_1 \rightarrow \psi_2\phi_2} u(p, \sigma), \quad (4.14)$$

where $\widehat{\mathcal{T}}_{\psi_1\phi_1 \rightarrow \psi_2\phi_2}$ has been calculated in Section 3 and the wave function renormalization constants of the involved fields are presented in Subsection 4.1. Within our working accuracy, the full amplitude should be truncated at $\mathcal{O}(p^3)$. Therefore, the chiral expansion of the full amplitude can be written as

$$\mathcal{T}_{\psi_1\phi_1 \rightarrow \psi_2\phi_2}(s, t) = \mathcal{T}_{\text{tree}}^{(1)} + \mathcal{T}_{\text{tree}}^{(2)} + \mathcal{T}_{\text{tree}}^{(3)} + \mathcal{T}_{\text{loop}}^{(3)} + \mathcal{T}_{\text{wf}}^{(3)}, \quad (4.15)$$

where the numbers in the superscripts denote the chiral orders. The last term is counted as $\mathcal{O}(p^3)$ and takes the form

$$\mathcal{T}_{\text{wf}}^{(3)} = \frac{1}{2} (\delta\mathcal{Z}_{\phi_1} + \delta\mathcal{Z}_{\psi_1} + \delta\mathcal{Z}_{\phi_2} + \delta\mathcal{Z}_{\psi_2}) \mathcal{T}_{\text{tree}}^{(1)}, \quad (4.16)$$

with $\delta\mathcal{Z}_{\phi_i} = \mathcal{Z}_{\phi_i} - 1$, $\delta\mathcal{Z}_{\psi_i} = \mathcal{Z}_{\psi_i} - 1$ ($i = 1, 2$). It is worth mentioning that this term perturbatively incorporates the effect of the multiplication of the wave function renormalization constants in Eq. (4.14), and the above procedure is usually called wave function renormalization. In another word, it actually takes into account the contribution of the diagrams with one-loop corrections on the external legs, as displayed in Figure 4.

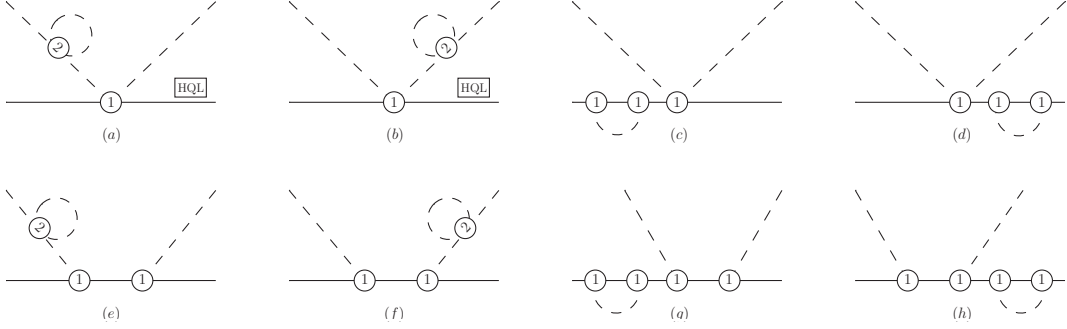


Figure 4. Loop diagrams of $\mathcal{O}(p^3)$ corresponding to wave function renormalization. Diagrams surviving in the HQL are indicated by boxed “HQL”.

The full scattering amplitude in Eq. (4.15) has UV divergencies and PCB terms. Here we adopt the EOMS scheme [55] to address these issues. The EOMS scheme contains two steps: $\overline{\text{MS}}-1$ subtraction and an extra finite renormalization.

In $\overline{\text{MS}}-1$ scheme, the bare baryon mass and axial-vector coupling constant, LECs are divided into renormalized and divergent parts. The divergent ones are used to cancel the UV divergence from loop amplitudes. To be specific, these quantities are written in the following form

$$\begin{aligned}
m &= m^r(\mu) + \beta_m \frac{R}{16\pi^2 F^2} , \\
g &= g^r(\mu) + \beta_g \frac{R}{16\pi^2 F^2} , \\
b_i &= b_i^r(\mu) + \beta_{b_i} \frac{R}{16\pi^2 F^2} \quad (i = 1, 2, \dots, 7) , \\
c_j &= c_j^r(\mu) + \beta_{c_j} \frac{R}{16\pi^2 F^2} \quad (j = 11, 12, \dots, 20) ,
\end{aligned} \tag{4.17}$$

where μ is the renormalization scale, and $R = 2/(d-4) - [\ln(4\pi) - \gamma_E + 1]$ with d being the number of space-time dimensions, $\gamma_E = 0.577216$ being the Euler constant. The UV β -functions are gathered in Appendix A.

Then we utilize a finite renormalization to restore the correct power counting. Since the PCB terms are polynomials of chiral expansion parameters, they can be properly absorbed by the LECs in the tree amplitudes. The EOMS-renormalized parameters are defined by

$$\begin{aligned}
m^r(\mu) &= \tilde{m} + \frac{\tilde{\beta}_m}{16\pi^2 F^2} , \\
g^r(\mu) &= \tilde{g} + \frac{\tilde{\beta}_g}{16\pi^2 F^2} ,
\end{aligned}$$

$$b_i^r(\mu) = \tilde{b}_i + \frac{\tilde{\beta}_{b_i}}{16\pi^2 F^2} \quad (i = 1, 2, \dots, 7) . \quad (4.18)$$

Here, the EOMS $\tilde{\beta}$ -functions are collected in Appendix B. Note that the $\mathcal{O}(p^3)$ LECs $c_j^r(\mu)$ maintain unchanged, i.e. $\tilde{c}_j = c_j^r$. The renormalized amplitudes obtained in EOMS scheme possess of original analytic structure and respect the power counting rule.

Finally, it should be mentioned that, in practical computations, the chiral limit decay constant F is always replaced by the physical decay constants, F_π , F_K and F_η . For the amplitude of the process $\psi_1\phi_1 \rightarrow \psi_2\phi_2$, this is achieved by making the following substitution

$$\frac{1}{F^{2n}} = \frac{1}{\left[\frac{F_{\phi_1}}{(1+\delta F_{\phi_1})}\right]^n \left[\frac{F_{\phi_2}}{(1+\delta F_{\phi_2})}\right]^n} = \frac{1}{F_{\phi_1}^n F_{\phi_2}^n} \left[1 + n(\delta F_{\phi_1} + \delta F_{\phi_2}) + \dots\right] . \quad (4.19)$$

It should be noted that such a substitution, when carried out for the $\mathcal{O}(p^1)$ tree amplitude, generates $\mathcal{O}(p^3)$ pieces that should be kept in our calculation. For the $\mathcal{O}(p^2)$ and $\mathcal{O}(p^3)$ amplitudes, one can merely make the replacement $F^{2n} \rightarrow (F_{\phi_1} F_{\phi_2})^n$, since the caused differences are of higher orders beyond the accuracy of our calculation. A merit of Eq. (4.19) is that the physical decay constants are properly chosen according to the incoming and outgoing Goldstone bosons. For instance, the F^2 in the amplitude of $\Xi_{cc}\pi \rightarrow \Xi_{cc}\pi$ is changed to F_π^2 rather than e.g. F_K^2 , while the one in the inelastic scattering amplitude of $\Xi_{cc}\pi \rightarrow \Xi_{cc}\eta$ is substituted by $F_\pi F_\eta$.

NLO expressions of the decay constants in ChPT can be found in Ref. [48], which read

$$F_{\phi_i} \equiv F(1 + \delta F_{\phi_i}) , \quad \phi_i \in \{\pi, K, \eta\} \quad (4.20)$$

with the chiral corrections being

$$\delta F_\pi = \frac{4m_\pi^2}{F^2}(L_4 + L_5) + \frac{8m_K^2}{F^2}L_4 + A_0(m_\pi^2) + \frac{1}{2}A_0(m_K^2) , \quad (4.21)$$

$$\delta F_K = \frac{4m_\pi^2}{F^2}L_4 + \frac{4m_K^2}{F^2}(2L_4 + L_5) + \frac{3}{8}A_0(m_\pi^2) + \frac{3}{4}A_0(m_K^2) + \frac{3}{8}A_0(m_\eta^2) , \quad (4.22)$$

$$\delta F_\eta = \frac{4(m_\pi^2 + 2m_K^2)}{F^2}L_4 + \frac{4m_\eta^2}{F^2}L_5 + \frac{3}{2}A_0(m_K^2) . \quad (4.23)$$

The bare parameters L_i 's are related to the corresponding UV-renormalized ones by

$$L_i = L_i^r(\mu) + \frac{\Gamma_i}{32\pi^2}R . \quad (4.24)$$

The Γ_i functions are given in Ref. [48] and are shown in Eq. (A.1) for easy reference.

5 Numerical results and discussions

5.1 Parameters

Masses and decay constants used in our work are collected in Table 6. Since the Ξ_{cc}^+ and Ξ_{cc}^{++} are treated as members of an isospin doublet, their masses are degenerate in the isospin limit and we take $m_{\Xi_{cc}} = 3621.55$ MeV from the PDG review [87]. Unlike the

Ξ_{cc} states, there is no experimental value for the Ω_{cc} baryon so far, therefore we employ $m_{\Omega_{cc}} = 3738$ MeV determined by lattice QCD [28].

For the decay constants of pion and kaon, we adopt their world-average values from Ref. [87]. It is known that the physical η and η' meson are superpositions of the singlet η_0 and octet η_8 , that can be systematically formulated in large- N_c ChPT, see e.g. Refs. [88, 89]. Nevertheless, in the standard SU(3) ChPT we are using here, the singlet η_0 is absent and the octet member η_8 is approximately regarded as the physical η meson. Based on the SU(3) ChPT calculation performed in Ref. [86], one has $F_\eta \simeq 1.27F_\pi \simeq 117$ MeV. This value is more or less in agreement with the recent lattice QCD determination [90], if one assumes $F_\eta \simeq F_\eta^8$ with $F^8 = 115.0$ MeV.

Table 6. Masses and decay constants used in our work. All the quantities in this table are in units of MeV.

	Goldstone	charm sector		decay constant	
m_π	139.57 [87]	$m_{\Xi_{cc}}$	3621.55 [87]	F_π	92.2 [87]
m_K	493.68 [87]	$m_{\Omega_{cc}}$	3738 [28]	F_K	112 [87]
m_η	547.86 [87]	m_D	1867 [87]	F_η	117
		m_{D_s}	1968 [87]		

Due to the lack of relevant experimental and lattice QCD data, a big challenge we encounter is the determination of the unknown LECs in the Lagrangians (3.10), (3.11) and (3.12). Thanks to the HDA symmetry [45], the doubly charmed baryon sector can be connected with the ones in the charmed meson sector. Derivation of the relations is detailed in Appendix D.

Specifically, for the LO coupling constant, one has

$$\tilde{g} = -\frac{1}{3\bar{m}_D}\tilde{g}_0, \quad (5.1)$$

where $\bar{m}_D = (m_D + m_{D_s})/2$ with m_D and m_{D_s} the physical masses of the D and D_s mesons, respectively. Here, \tilde{g}_0 denotes the axial coupling constant of the $D^*D\phi$ interaction, c.f. Eq. (D.5). Its value can be fixed via the LO calculation of the decay width of $D^{*+} \rightarrow D^0\pi$ [87], which leads to $\tilde{g}_0 \simeq 1.095$ GeV. For the $O(p^2)$ LECs, one obtains

$$\begin{aligned} \tilde{b}_1 &= -\frac{1}{2\bar{m}_D}(\tilde{h}_0 + \frac{1}{3}\tilde{h}_1), & \tilde{b}_2 &= -\frac{1}{2\bar{m}_D}\tilde{h}_1, & \tilde{b}_3 &= -\frac{1}{2\bar{m}_D}\tilde{h}_3, \\ \tilde{b}_4 &= \frac{1}{2\bar{m}_D}\tilde{h}_2, & \tilde{b}_5 &= \frac{\bar{m}_D}{8}\tilde{h}_5, & \tilde{b}_6 &= -\frac{\bar{m}_D}{8}\tilde{h}_4. \end{aligned} \quad (5.2)$$

At $O(p^3)$, the following pertinent relations are established,

$$\tilde{c}_{11} = \frac{\tilde{g}_2}{2}, \quad \tilde{c}_{12} = \frac{\bar{m}_D^2}{4}\tilde{g}_3, \quad \tilde{c}_{20} = -\frac{\tilde{g}_1}{2}. \quad (5.3)$$

The parameters $\tilde{h}_{0,1,\dots,5}$ in Eq. (5.2) and $\tilde{g}_{1,2,3}$ in Eq. (5.3) are the LECs involved in the NLO and NNLO effective Lagrangians, respectively, that describe the interactions between the

NGBs and charmed mesons; see Eq. (D.6) and Eq. (D.7) in Appendix D. Their values have been determined by fitting to lattice QCD data in Ref. [72]. Therein, four different fits were performed using the method of unitarized ChPT (UChPT). The fit denoted by UChPT-6(b') was done by enforcing the naturalness requirements of the fitting parameters. Moreover, the validity range of UChPT is ensured by further excluding the lattice data with a pion mass larger than 600 MeV. As it was expected, the obtained $D\phi$ LECs from the UChPT-6(b') fit are more natural than the others in Ref. [72]. Therefore we utilize the UChPT-6(b') outputs, collected in the last column of Table 7 for completeness, to estimate the values of \tilde{b}_i ($i = 1, \dots, 6$) and \tilde{c}_i ($i = 11, 12, 20$). The obtained results are shown in the 2nd column of Table 7. Importantly, those LECs determined by HDA symmetry are acceptable in the sense that they turn out to be of natural size. Furthermore, the corresponding uncertainties are obtained by Monte Carlo propagating the errors of the $D\phi$ LECs of Ref. [72].⁴

Table 7. Values of the LECs determined by making use of HDA symmetry. The LECs b_i 's and c_j 's are in units of GeV^{-1} and GeV^{-2} , respectively.

$\psi\phi$ scattering		$D\phi$ scattering [72]	
LECs	Value	LECs	Value
\tilde{g}	-0.19	\tilde{g}_0	1.095
\tilde{b}_1	-0.04	\tilde{h}_0	0.0172
\tilde{b}_2	-0.11	\tilde{h}_1	0.4266
\tilde{b}_3	$-1.46^{+0.43}_{-0.46}$	\tilde{h}_3	$5.59^{+2.07}_{-1.96}$
\tilde{b}_4	0.66 ± 0.19	\tilde{h}_2	$2.52^{+0.73}_{-0.74}$
\tilde{b}_5	$-0.17^{+0.05}_{-0.06}$	\tilde{h}_5	$-0.71^{+0.23}_{-0.24}$
\tilde{b}_6	0.11 ± 0.04	\tilde{h}_4	$-0.47^{+0.17}_{-0.17}$
\tilde{c}_{11}	$-0.08^{+0.21}_{-0.14}$	\tilde{g}_2	$-0.16^{+0.52}_{-0.39}$
\tilde{c}_{12}	$0.08^{+0.03}_{-0.02}$	\tilde{g}_3	$0.08^{+0.03}_{-0.03}$
\tilde{c}_{20}	$0.49^{+0.09}_{-0.15}$	\tilde{g}_1	$-0.99^{+0.30}_{-0.18}$

It is worth noting that \tilde{h}_1 in Table 7 was fixed by the mass difference between D and D_s mesons in Ref. [72]. Likewise, in our case the LEC \tilde{b}_2 can be estimated by the mass difference of the Ξ_{cc} and Ω_{cc} baryons. With the help of Eq. (4.7) and Eq. (4.8), one obtains

$$\tilde{b}_2 \simeq \frac{m_{\Xi_{cc}} - m_{\Omega_{cc}}}{4(m_K^2 - m_\pi^2)} \simeq -0.13 \text{ GeV}^{-1}. \quad (5.4)$$

⁴Specifically, sample groups of random values of the $D\phi$ LECs are generated by Monte Carlo method with normal distribution [91]. The MINOS algorithm in the package Minuit [92] is followed to select good samples of normally-distributed parameters that satisfy the condition $\chi^2 - \chi_{\min}^2 \leq 1$. Here, χ^2 and χ_{\min}^2 are calculated by using the randomly-generated parameters and the central values of the $D\phi$ LECs, respectively. A sufficient number of simulations have been performed, leading to 156 groups of good values of the $D\phi$ LECs. The 156 sets of parameter values are then utilized to estimate the uncertainties of the LECs in the doubly charmed baryon sector with the help of the HDA-symmetry relations (5.2) and (5.3). Moreover, the errors of scattering lengths and phase shifts to be discussed in the next subsections are propagated from the uncertainties of the $\psi\phi$ LECs.

Mention that the loop corrections have been neglected and the masses in Table 6 have been used. One can see that the \tilde{b}_2 value in Eq. (5.4) is comparable with the one in Table 7, justifying the validity of HDA symmetry to a certain extent.

In fact, a more reliable determination of \tilde{b}_1 and \tilde{b}_2 has been conducted in Ref. [63]. The two LECs are pinned down by fitting to the lattice QCD data of the baryon masses, leading to⁵

$$\tilde{b}_1 = -0.09 \pm 0.08 \text{ GeV}^{-1}, \quad \tilde{b}_2 = -0.09 \pm 0.09 \text{ GeV}^{-1}. \quad (5.5)$$

The \tilde{b}_1 - \tilde{b}_2 parameter space allowed by 1- σ uncertainties cover the values of \tilde{b}_1 and \tilde{b}_2 in Table 7 and Eq. (5.4). Therefore, we use Eq. (5.5) for \tilde{b}_1 and \tilde{b}_2 throughout this paper. It should be also stressed that the numbers in Eq. (5.5) are obtained at the renormalization scale $\mu = 1 \text{ GeV}$. For consistency, the same renormalization scale is chosen, during our numerical computation of one-loop corrections.

Apart from the fixed parameters discussed above, there are still eight unknown LECs. Since they can not be estimated via HDA symmetry, we assume them to be zero, $\tilde{b}_7 = 0.0 \text{ GeV}^{-1}$ and $\tilde{c}_k = 0.0 \text{ GeV}^{-2}$, $k \in \{13, \dots, 19\}$. Such an assumption is more or less reasonable in view of the smallness for most of the LECs in Table 7. A solid determination of these parameters is expected to be done only when lattice QCD data of e.g. scattering lengths are available in the future.

Finally, the values of the LECs L_4^r and L_5^r can be found in Ref [48], $L_4^r = -0.3 \times 10^{-3}$ and $L_5^r = 1.4 \times 10^{-3}$, which are obtained at the scale $\mu = M_\rho$. An recent update of the mesonic LECs is summarized in Ref. [93], and comparable results of L_4^r and L_5^r are achieved. Those values at $\mu = M_\rho$ can be translated to the ones at $\mu = 1 \text{ GeV}$ with the help of the following relations

$$L_i^r(\mu) = L_i^r(M_\rho) + \frac{\Gamma_i}{16\pi^2} \ln\left(\frac{M_\rho}{\mu}\right). \quad (5.6)$$

5.2 Prediction of scattering lengths

Once all the involved LECs are pinned down, we are now in the position to calculate the S - and P -wave scattering lengths numerically. By definition, scattering lengths can be calculated via

$$a_{\ell\pm} = \lim_{|\mathbf{q}|\rightarrow 0} \frac{f_{\ell\pm}(s)}{\mathbf{q}^{2\ell}}. \quad (5.7)$$

However, the fraction on right hand side can not be computed numerically exact at threshold for $\ell \geq 1$. That is, the fraction value becomes undefined when one has zeros in the denominator, as the modulus of the three momentum is vanishing. To avoid this issue, by making use of Eq. (2.33), we have derived analytical expressions for the S - and P -wave scattering lengths, with which numerical computations can be carried out precisely. For calculations with accuracy up to NNLO, derivatives of one-loop integrals are involved, which are handled by adopting the techniques proposed in Ref. [94].

⁵The LECs b_1 and b_2 are related to the ones used in Ref. [63] via $b_1 = \hat{c}_1 + \frac{1}{3}c_7$ and $b_2 = c_7$.

Table 8. S -wave scattering lengths $a_{0+}^{(S,I)}$ ($J^P = \frac{1}{2}^-$) in units of fm.

(S, I)	Processes	$\mathcal{O}(p^1)$	$\mathcal{O}(p^2)$	$\mathcal{O}(p^3)$		Total	Ref. [67]
				Tree	Loop		
$(-2, \frac{1}{2})$	$\Omega_{cc}\bar{K} \rightarrow \Omega_{cc}\bar{K}$	-0.27	0.29	-0.11	-0.001	$-0.09_{-0.13}^{+0.12}$	-0.20(1)
$(1, 1)$	$\Xi_{cc}K \rightarrow \Xi_{cc}K$	-0.27	0.27	-0.13	-0.47	-0.60 ± 0.13	-0.25(1)
$(1, 0)$	$\Xi_{cc}K \rightarrow \Xi_{cc}K$	0.27	0.34	0.13	0.30	1.03 ± 0.19	0.92(2)
$(0, \frac{3}{2})$	$\Xi_{cc}\pi \rightarrow \Xi_{cc}\pi$	-0.12	0.04	-0.01	-0.06	-0.16 ± 0.02	-0.10(2)
$(-1, 0)$	$\Xi_{cc}\bar{K} \rightarrow \Xi_{cc}\bar{K}$	0.54	0.24	0.25	0.16	$1.19_{-0.21}^{+0.22}$	2.15(11)
	$\Omega_{cc}\eta \rightarrow \Omega_{cc}\eta$	-0.001	0.37	0.0	$0.05 + 0.55i$	$0.42_{-0.19}^{+0.18} + 0.55i$	$0.57(3) + 0.21i$
$(-1, 1)$	$\Omega_{cc}\pi \rightarrow \Omega_{cc}\pi$	0.0	0.04	0.0	-0.04	-0.01 ± 0.02	-0.002(1)
	$\Xi_{cc}\bar{K} \rightarrow \Xi_{cc}\bar{K}$	0.0	0.31	0.0	$-0.04 + 0.10i$	$0.27_{-0.13}^{+0.13} + 0.10i$	$0.26(1) + 0.19i$
$(0, \frac{1}{2})$	$\Xi_{cc}\pi \rightarrow \Xi_{cc}\pi$	0.25	0.04	0.01	0.04	0.34 ± 0.02	0.36(1)
	$\Xi_{cc}\eta \rightarrow \Xi_{cc}\eta$	-0.001	0.32	0.0	-0.26	$0.06_{-0.15}^{+0.14}$	$0.34(1) + 0.10i$
	$\Omega_{cc}K \rightarrow \Omega_{cc}K$	0.27	0.29	0.11	$-0.01 + 0.55i$	$0.66_{-0.13}^{+0.13} + 0.55i$	$1.18(6) + 0.29i$

Results of the S -wave scattering lengths with quantum numbers $J^P = \frac{1}{2}^-$ are collected in Table 8. The uncertainties are propagated from the errors of the LECs by means of Monte Carlo methodology. We are concerning ourselves only with the 11 elastic scattering processes that are indicated by the first and second columns of Table 8. Contributions from $\mathcal{O}(p^1)$, $\mathcal{O}(p^2)$, $\mathcal{O}(p^3)$ trees, $\mathcal{O}(p^3)$ loops and their sum are displayed separately. The $\mathcal{O}(p^1)$ S -wave scattering lengths are dominated by the contributions from the WT term, without any unknown LECs. The contributions of baryon-exchanging diagrams are suppressed. The explicit expressions of the NLO S -wave scattering lengths do not contain b_7 , while the other NLO LECs b_i ($i = 1, \dots, 6$) are well fixed by HDA symmetry. On the contrary, the $\mathcal{O}(p^3)$ tree contributions are roughly estimated due to the fact that, except for c_{11} , c_{12} and c_{20} , most of the NNLO LECs are simply set to zero.

The convergence of SU(3) ChPT has remained under debate for over several decades, see e.g. Refs. [56]. Generally speaking, the convergence in the three-flavor ChPT calculations is usually worse than the two-flavor case, due to the relatively large strange quark mass.⁶ Here it would be also interesting to have a look at the convergence properties of the chiral expansion of the $\psi\phi$ scattering lengths. We first discuss the processes involving pion mesons. It can be seen from Table 8 that the chiral series for the elastic $\Xi_{cc}\pi$ scatterings, with $(S, I) = (0, 3/2)$ or $(0, 1/2)$, converge well if one only concerns the first two orders. Namely, the $\mathcal{O}(p^1)$ contributions are significantly larger than the $\mathcal{O}(p^2)$ ones. Nevertheless, although the sums of $\mathcal{O}(p^3)$ trees and loops in the two channels are small, there are comparable to the $\mathcal{O}(p^2)$ trees. We ascribe the failure of convergence to the underestimation of the $\mathcal{O}(p^3)$ trees for poor information on the LECs. As for $\Omega_{cc}\pi \rightarrow \Omega_{cc}\pi$, scattering length starts to

⁶It should be pointed out that a one-loop calculation is not really sufficient to make a solid statement about convergence. It is well-known from both mesonic and baryonic sectors of ChPT that one needs at least two loops to make a significant statement about the chiral expansion. For example, an estimate for the convergence radius of the chiral expansion of the nucleon mass at the two-loop level was performed in Refs. [95, 96], indicating a breakdown of convergence already below $m_\pi \approx 360$ MeV. The convergence might be even worse in the SU(3) case, since the kaons and the eta are substantially heavier.

contribute at $O(p^2)$, since the LO term for this channel (see Eq. (3.14) and Table 1) is identical to zero exactly.

On the other hand, the scatterings of kaon and eta mesons off doubly charmed baryons have bad convergence properties, due to the emergence of large masses of kaon and eta as chiral expansion parameters. Such a non-convergent behaviour usually implies resummation of diagrams is required so that higher-order contributions can be implemented non-perturbatively. Similar situations happened for SU(3) meson-meson scatterings [86], and kaon-nucleon scatterings [97, 98]. In general, the resummation procedure restores unitarity and extends the applicability range of ChPT, see Refs. [29] for a recent review. It should be emphasized that, the so-called UChPT amplitude plays a crucial role in investigating the spectrum of doubly charmed baryons. For instance, possible candidates of negative-parity doubly charmed baryons have been found on the basis of the LO [65] and NLO [66] ChPT amplitudes. It is also worth noting that the $O(p^3)$ amplitudes turn out to be significant and an inclusion of their effects may improve the studies made in Refs. [65, 66]. Especially for the two channels, $\Xi_{cc}K \rightarrow \Xi_{cc}K$ with $(S, I) = (1, 1)$ and $\Omega_{cc}\bar{K} \rightarrow \Omega_{cc}\bar{K}$ with $(S, I) = (-2, 1/2)$, since there exist large cancellations between the LO and NLO contributions, the NNLO corrections become dominating. In a word, the ChPT amplitudes up to NNLO, we obtain in this work, can be applied to systematically scrutinize the doubly-charmed-baryon spectroscopy in the future, once more experimental or lattice QCD data are available.

For comparison, the HB results of Ref. [67] are shown in the last column of Table 8. For all the channels, our relativistic results are qualitatively consistent with the ones obtained in the HB formalism. Relativistic corrections are mainly responsible for the differences. Another source might be owing to the fact that the HQL-vanishing diagrams are not taken into account in the calculation of Ref. [67]. Nevertheless, their contributions are negligible, which will be illustrated below. Lastly, the spin-3/2 doubly charmed baryons are incorporated as explicit degrees of freedom in Ref. [67], which would lead to discrepancies as well. As we can see, good agreements are observed within one-sigma uncertainties for the five channels: $\Omega_{cc}\bar{K}$ with $(S, I) = (-2, 1/2)$, $\Xi_{cc}K$ with $(S, I) = (1, 0)$, $\Omega_{cc}\eta$ with $(S, I) = (-1, 0)$, $\Omega_{cc}\pi$ with $(S, I) = (-1, 1)$ and $\Xi_{cc}\pi$ with $(S, I) = (0, 1/2)$. Such an observation implies that the net effects of relativistic corrections, contributions of HQL-vanishing diagrams and resonance-exchanging diagrams are slight for those channels in S wave.

P -wave scattering lengths with $J^P = \frac{3}{2}^+$ and $J^P = \frac{1}{2}^+$ are compiled in Table 9 and Table 10, respectively. It is found that, at $O(p^1)$, the P -wave scattering lengths are entirely saturated by the crossing partner of diagram (a). For some channels like $\Xi_{cc}\pi$ scatterings, contributions from $O(p^3)$ loops to the P -wave scattering lengths turn out to be sizeable.

Before ending this subsection, we intend to discuss the contributions of HQL-surviving diagrams in more detail. In the HQL, most of the diagrams in Figures 1, 2 and 4 do not contribute at threshold. This can be illustrated by performing an expansion in terms of the inverse of the baryon mass, i.e. HB projection. For the axial term in Eq. (3.10), the HB projection yields

$$\bar{\psi} \left\{ \frac{g}{2} \not{u} \gamma_5 \right\} \psi \longrightarrow \bar{\mathcal{N}}_v \{ g S_\nu \cdot u \} \mathcal{N}_v + \alpha_1 m^{-1} + \alpha_2 m^{-2} + \dots \quad (5.8)$$

Table 9. P -wave scattering lengths $a_{1+}^{(S,I)}$ ($J^P = \frac{3}{2}^+$) in units of 10^{-2} fm^3 .

(S, I)	Processes	$\mathcal{O}(p^1)$	$\mathcal{O}(p^2)$	$\mathcal{O}(p^3)$		Total
				Tree	Loop	
$(-2, \frac{1}{2})$	$\Omega_{cc}\bar{K} \rightarrow \Omega_{cc}\bar{K}$	0.16	0.60	-0.22	-3.00	$-2.47^{+3.04}_{-2.64}$
$(1, 1)$	$\Xi_{cc}K \rightarrow \Xi_{cc}K$	0.10	0.59	-0.22	-1.19	$-0.73^{+3.02}_{-2.64}$
$(1, 0)$	$\Xi_{cc}K \rightarrow \Xi_{cc}K$	-0.10	-8.77	0.22	1.71	$-6.93^{+2.83}_{-3.21}$
$(0, \frac{3}{2})$	$\Xi_{cc}\pi \rightarrow \Xi_{cc}\pi$	0.62	0.75	-0.18	-41.8	$-40.6^{+3.20}_{-2.97}$
$(-1, 0)$	$\Xi_{cc}\bar{K} \rightarrow \Xi_{cc}\bar{K}$	0.0	5.27	0.45	0.48	$6.19^{+4.78}_{-5.40}$
	$\Omega_{cc}\eta \rightarrow \Omega_{cc}\eta$	0.07	2.0	0.0	$-1.13 + 0.01i$	$0.93^{+2.04}_{-1.96} + 0.01i$
$(-1, 1)$	$\Omega_{cc}\pi \rightarrow \Omega_{cc}\pi$	0.0	-6.23	0.001	-0.10	$-6.32^{+1.85}_{-1.82}$
	$\Xi_{cc}\bar{K} \rightarrow \Xi_{cc}\bar{K}$	0.0	-4.09	0.0	$-0.11 + 0.01i$	$-4.2^{+1.23}_{-1.21} + 0.01i$
$(0, \frac{1}{2})$	$\Xi_{cc}\pi \rightarrow \Xi_{cc}\pi$	-0.31	0.75	0.35	21.2	$21.9^{+3.39}_{-3.70}$
	$\Xi_{cc}\eta \rightarrow \Xi_{cc}\eta$	0.02	-2.31	0.0	$-0.01 + 0.01i$	$-2.30^{+1.13}_{-1.13} + 0.01i$
	$\Omega_{cc}K \rightarrow \Omega_{cc}K$	0.0	0.6	0.22	$0.19 + 0.01i$	$1.0^{+2.67}_{-3.01} + 0.01i$

Table 10. P -wave scattering lengths $a_{1-}^{(S,I)}$ ($J^P = \frac{1}{2}^+$) in units of 10^{-2} fm^3 .

(S, I)	Processes	$\mathcal{O}(p^1)$	$\mathcal{O}(p^2)$	$\mathcal{O}(p^3)$		Total
				Tree	Loop	
$(-2, \frac{1}{2})$	$\Omega_{cc}\bar{K} \rightarrow \Omega_{cc}\bar{K}$	-0.38	0.58	-0.34	0.02	$-0.13^{+3.03}_{-2.64}$
$(1, 1)$	$\Xi_{cc}K \rightarrow \Xi_{cc}K$	-0.36	0.57	-0.37	-1.74	$-1.90^{+3.01}_{-2.61}$
$(1, 0)$	$\Xi_{cc}K \rightarrow \Xi_{cc}K$	0.36	-8.80	0.37	0.46	$-7.59^{+2.82}_{-3.20}$
$(0, \frac{3}{2})$	$\Xi_{cc}\pi \rightarrow \Xi_{cc}\pi$	-0.80	0.75	-0.2	19.5	$19.3^{+3.19}_{-2.97}$
$(-1, 0)$	$\Xi_{cc}\bar{K} \rightarrow \Xi_{cc}\bar{K}$	0.16	5.25	0.74	-9.77	$-3.61^{+4.77}_{-5.37}$
	$\Omega_{cc}\eta \rightarrow \Omega_{cc}\eta$	-0.13	1.97	0.0	$-2.16 + 0.01i$	$-0.32^{+2.03}_{-1.95} + 0.01i$
$(-1, 1)$	$\Omega_{cc}\pi \rightarrow \Omega_{cc}\pi$	0.0	-6.23	0.0	-0.53	$-6.75^{+1.85}_{-1.82}$
	$\Xi_{cc}\bar{K} \rightarrow \Xi_{cc}\bar{K}$	0.0	-4.11	0.0	$-0.60 + 0.01i$	$-4.72^{+1.24}_{-1.22} + 0.01i$
$(0, \frac{1}{2})$	$\Xi_{cc}\pi \rightarrow \Xi_{cc}\pi$	-0.27	0.75	0.39	-104.9	$-104.1^{+3.38}_{-3.70}$
	$\Xi_{cc}\eta \rightarrow \Xi_{cc}\eta$	-0.03	-2.33	0.0	$-1.43 + 0.01i$	$-3.79^{+1.13}_{-1.14} + 0.01i$
	$\Omega_{cc}K \rightarrow \Omega_{cc}K$	0.16	0.58	0.34	$-3.77 + 0.01i$	$-2.69^{+2.67}_{-3.00} + 0.01i$

where the spin matrix is $S_v^\mu \equiv \frac{i}{2}\gamma_5\sigma^{\mu\nu}v_\nu$ with the four vector $v^\mu = (1, 0, 0, 0)$. In the HQL, $m \rightarrow \infty$, all the inverse mass terms approach to zero. Only the first term that is independent of mass survives. However, it vanishes at threshold due to the feature of derivative coupling of the NGBs. Specifically, one has

$$\bar{\mathcal{N}}_v \{gS_v \cdot u\} \mathcal{N}_v \propto \bar{\mathcal{N}}_v \{gS_v \cdot \partial\phi\} \mathcal{N}_v \quad (5.9)$$

which corresponds to $S_v \cdot q_\phi$ in the momentum space, with q_ϕ being the momentum of Goldstone boson. At threshold, $q_\phi = (m_\phi, \vec{0})$, leading to $S_v \cdot q_\phi = 0$. Subsequently, all the

diagrams containing axial vertices disappear in the HQL. Therefore, only the diagrams that are irrelevant to the axial coupling g survive. For easy reference, they have been labelled by boxed "HQL" in Figures 1, 2 and 4.

Results of scattering lengths obtained by including only the HQL-surviving diagrams are shown in Table 11. As expected, for the S -wave scattering lengths the deviation of the HQL results in Table 11 from the ones in Table 8 is negligible. However, the results of P -wave scattering lengths change dramatically by switching off the HQL-vanishing diagrams, especially for a_{1+} with $J^P = \frac{3}{2}^+$. One may probably ascribe such large variations to the absence of the HQS partners like spin-3/2 doubly charmed baryons. They are expected to contribute equally as the spin-3/2 baryons, since the HQS symmetry is exact in HQL. In the next subsection, we will evaluate the effect of the spin-3/2 doubly charmed baryons.

Table 11. Results of scattering lengths obtained by taking only the HQL-surviving diagrams into consideration. The S - and P -wave scattering lengths are in units of fm and 10^{-2} fm^3 , respectively.

(S, I)	Processes	$a_{0+} [J^P = \frac{1}{2}^-]$	$a_{1+} [J^P = \frac{3}{2}^+]$	$a_{1-} [J^P = \frac{1}{2}^+]$
$(-2, \frac{1}{2})$	$\Omega_{cc}\bar{K} \rightarrow \Omega_{cc}\bar{K}$	$-0.08^{+0.12}_{-0.13}$	$0.34^{+3.04}_{-2.64}$	$-1.42^{+3.03}_{-2.64}$
$(1, 1)$	$\Xi_{cc}K \rightarrow \Xi_{cc}K$	-0.62 ± 0.13	$0.39^{+3.02}_{-2.62}$	$-2.51^{+3.01}_{-2.61}$
$(1, 0)$	$\Xi_{cc}K \rightarrow \Xi_{cc}K$	1.03 ± 0.19	$-8.19^{+2.83}_{-3.21}$	$-7.41^{+2.82}_{-3.20}$
$(0, \frac{3}{2})$	$\Xi_{cc}\pi \rightarrow \Xi_{cc}\pi$	-0.15 ± 0.02	$0.63^{+3.20}_{-2.97}$	$-1.26^{+3.19}_{-2.97}$
$(-1, 0)$	$\Xi_{cc}\bar{K} \rightarrow \Xi_{cc}\bar{K}$	$1.19^{+0.22}_{-0.21}$	$6.36^{+4.78}_{-5.40}$	$4.66^{+4.77}_{-5.37}$
	$\Omega_{cc}\eta \rightarrow \Omega_{cc}\eta$	$0.42^{+0.18}_{-0.19} + 0.56i$	$2.03^{+2.04}_{-1.96}$	$-0.12^{+2.03}_{-1.95} + 0.02i$
$(-1, 1)$	$\Omega_{cc}\pi \rightarrow \Omega_{cc}\pi$	0.0 ± 0.02	$-6.23^{+1.85}_{-1.82}$	$-6.72^{+1.85}_{-1.82}$
	$\Xi_{cc}\bar{K} \rightarrow \Xi_{cc}\bar{K}$	$0.28^{+0.13}_{-0.13} + 0.10i$	$-4.14^{+1.23}_{-1.21}$	$-4.71^{+1.24}_{-1.22}$
$(0, \frac{1}{2})$	$\Xi_{cc}\pi \rightarrow \Xi_{cc}\pi$	0.33 ± 0.02	$1.41^{+3.39}_{-3.70}$	$1.51^{+3.38}_{-3.70}$
	$\Xi_{cc}\eta \rightarrow \Xi_{cc}\eta$	$0.05^{+0.14}_{-0.15}$	-2.16 ± 1.13	$-3.32^{+1.13}_{-1.14}$
	$\Omega_{cc}K \rightarrow \Omega_{cc}K$	$0.64^{+0.13}_{-0.13} + 0.55i$	$1.14^{+2.67}_{-3.01}$	$-1.01^{+2.67}_{-3.00} + 0.03i$

5.3 Effect of spin-3/2 doubly charmed baryons

According to the naive quark model with flavour SU(4) (u, d, s, c quarks) symmetry, there are three ground 20-plets, i.e. $\mathbf{4} \otimes \mathbf{4} \otimes \mathbf{4} = \mathbf{20}_S \oplus \mathbf{20}_M \oplus \mathbf{20}_M \oplus \mathbf{4}_A$. The spin-1/2 doubly charmed baryons, Ξ_{cc}^{++} , Ξ_{cc}^+ and Ω_{cc}^+ , belong to one of the mixed-symmetric 20-plets, while the spin-3/2 doubly charmed baryons, $\Xi_{cc}^{\prime++}$, $\Xi_{cc}^{\prime+}$ and $\Omega_{cc}^{\prime+}$, to the symmetric 20-plet $\mathbf{20}_S$; See e.g. Ref. [99] for a detailed review. In the HQL, the two doubly-charmed-baryon triplets degenerate and should be treated on equal footing, c.f. Eq. (D.2), in line with HQS symmetry [100]. In this sense, the effects of spin-3/2 baryons are as important as those of the spin-1/2 ones. Therefore, in this subsection, we aim to assess the impact of spin-3/2 doubly charmed baryons on the scattering lengths within the framework of covariant BChPT.

The inclusion of spin-3/2 baryons in covariant BChPT is complicated. An appropriate power counting rule should be assigned to the new parameter, i.e. the mass difference

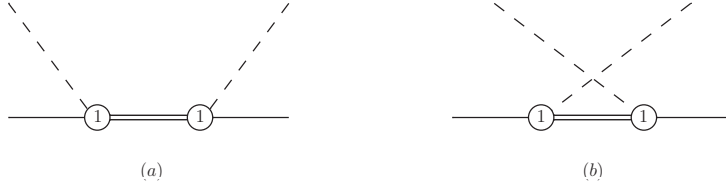


Figure 5. Tree diagrams contributing to $\psi\phi$ scattering at LO. The solid, dashed and double lines represent the spin-1/2 baryons, the pions and the spin-3/2 doubly baryons, in order.

between the spin-1/2 and spin-3/2 baryons, denoted by Δ hereafter. Like the treatment of the $\Delta(1232)$ resonances in the traditional BChPT, here we adopt the so-called δ -counting rule that was proposed in Ref. [102]. Specifically, in the energy region near threshold the mass splitting Δ is counted as $O(p^{1/2})$ in addition to Eq. (3.2). According to this power counting rule, the spin-3/2 baryon propagator is $O(p^{-1/2})$. Loops with internal spin-3/2 baryon lines are at least of order $O(p^{7/2})$, and therefore their contributions are beyond the accuracy of our calculation. For the calculation up to $O(p^3)$, we only need to take into account the LO and NLO tree-level contributions from explicit spin-3/2 baryons, which are $O(p^{3/2})$ and $O(p^{5/2})$, respectively. In order to avoid the emergence of too many new unknown LECs, the NLO Born-term contribution is omitted here. In fact, as pointed out in Ref. [103], the NLO Born term is redundant in the sense that its contribution can be absorbed by redefining the coupling h_A in the LO Born term (see Eq. (5.12)) and the LECs in the contact terms (3.16) and (3.18).

For the purpose of our calculation the following LO Lagrangian are needed,

$$\begin{aligned} \mathcal{L}_{\frac{3}{2}} = & -\bar{\psi}'^\mu [g_{\mu\nu}(i\not{D} - M) + iA(\gamma_\mu D_\nu + \gamma_\nu D_\mu) + \frac{i}{2}(3A^2 + 2A + 1)\gamma_\mu \not{D} \gamma_\nu \\ & + M(3A^2 + 3A + 1)\gamma_\mu \gamma_\nu] \psi'^\nu + \frac{h_A}{2} (\bar{\psi} u^\mu \psi'_\mu + H.c.) , \end{aligned} \quad (5.10)$$

where M and h_A are the mass of the spin-3/2 baryons and the coupling constant of the $\psi\psi'\phi$ interactions in the chiral limit, respectively. A is an arbitrary real parameter but $A \neq -1/2$. The spin-3/2 doubly charmed baryons are collected in the triplet

$$\psi'_\mu = \begin{pmatrix} \Xi_{cc}'^{++} \\ \Xi_{cc}'^+ \\ \Omega_{cc}'^+ \end{pmatrix}_\mu . \quad (5.11)$$

Feynman diagrams relevant to our calculation are displayed in Figure 5. Tree-level amplitudes are derived, which can be written in the form as

$$\begin{aligned} \mathcal{A}_{\text{tree}}^{(1)} = & -\frac{h_A^2}{48F^2} [\mathcal{C}_S^{(1)} \mathcal{F}'(s) + \mathcal{C}_U^{(1)} \mathcal{F}'(u)] , \\ \mathcal{B}_{\text{tree}}^{(1)} = & \frac{h_A^2}{24F^2} [\mathcal{C}_S^{(1)} \mathcal{G}'(s) - \mathcal{C}_U^{(1)} \mathcal{G}'(u)] , \end{aligned} \quad (5.12)$$

where the coefficients $\mathcal{C}_S^{(1)}$ and $\mathcal{C}_U^{(1)}$ are the same as those in Eq. (3.14), which are shown in Table 1. Nevertheless, the exchanged spin-1/2 baryons indicated in Table 1 should be

substituted by their spin-3/2 partners. Explicit expressions of the functions \mathcal{F}' and \mathcal{G}' are given by

$$\begin{aligned}
\mathcal{F}'(s) &= \frac{1}{M^2(s-M^2)} \left\{ (m_{\psi_1} + m_{\psi_2})(m_{\psi_1}^2 - m_{\phi_1}^2 - s)(m_{\psi_2}^2 - m_{\phi_2}^2 - s) \right. \\
&\quad - M[(m_{\psi_1} - m_{\psi_2})^2(m_{\psi_1}m_{\psi_2} + s) - m_{\psi_1}m_{\psi_2}(m_{\phi_1}^2 + m_{\phi_2}^2) - 2s(m_{\phi_1}^2 + m_{\phi_2}^2) \\
&\quad + 3(m_{\psi_2}^2m_{\phi_1}^2 + m_{\psi_1}^2m_{\phi_2}^2) - 4m_{\phi_1}^2m_{\phi_2}^2] - M^2[(m_{\psi_1}^2 + m_{\psi_2}^2 - 2s - 3t)(m_{\psi_1} + m_{\psi_2}) \\
&\quad + 2m_{\psi_2}(2m_{\phi_1}^2 + m_{\phi_2}^2) + 2m_{\psi_1}(m_{\phi_1}^2 + 2m_{\phi_2}^2)] \\
&\quad \left. - 2M^3[m_{\psi_1}^2 + m_{\psi_2}^2 + 3(m_{\phi_1}^2 + m_{\phi_2}^2 - t) - 2s] \right\}, \\
\mathcal{G}'(s) &= \frac{1}{M^2(s-M^2)} \left\{ 2M^3(m_{\psi_1} + m_{\psi_2}) - (m_{\psi_1}^2 - m_{\phi_1}^2 - s)(m_{\psi_2}^2 - m_{\phi_2}^2 - s) \right. \\
&\quad + M[m_{\psi_2}(m_{\psi_1}^2 - m_{\phi_1}^2 - s) + m_{\psi_1}(m_{\psi_2}^2 - m_{\phi_2}^2 - s)] \\
&\quad \left. + M^2[(m_{\psi_1} + m_{\psi_2})^2 + 2(m_{\phi_1}^2 + m_{\phi_2}^2) - 3t] \right\}. \tag{5.13}
\end{aligned}$$

As argued in Ref. [101], physical quantities are independent of the parameter A . Therefore, we have set $A = -1$ for convenience as done in Ref. [103].

Table 12. LO contributions of the spin-3/2 ψ' baryons to the scattering lengths. Δ denotes the mass difference between the spin-3/2 and spin-1/2 baryons. The S - and P -wave scattering lengths are in units of fm and 10^{-2} fm³, respectively.

(S, I)	Processes	$\Delta = 50$ MeV			$\Delta = 100$ MeV			$\Delta = 150$ MeV		
		a_{0+}	a_{1+}	a_{1-}	a_{0+}	a_{1+}	a_{1-}	a_{0+}	a_{1+}	a_{1-}
$(-2, \frac{1}{2})$	$\Omega_{cc}\bar{K} \rightarrow \Omega_{cc}\bar{K}$	-0.02	0.31	1.25	-0.02	0.28	1.11	-0.02	0.25	1.00
$(1, 1)$	$\Xi_{cc}K \rightarrow \Xi_{cc}K$	-0.02	0.19	0.80	-0.02	0.18	0.74	-0.02	0.17	0.69
$(1, 0)$	$\Xi_{cc}K \rightarrow \Xi_{cc}K$	0.02	-0.19	-0.80	0.02	-0.18	-0.74	0.02	-0.17	-0.69
$(0, \frac{3}{2})$	$\Xi_{cc}\pi \rightarrow \Xi_{cc}\pi$	-0.003	0.94	3.79	-0.003	0.75	2.99	-0.003	0.61	2.47
$(-1, 0)$	$\Xi_{cc}\bar{K} \rightarrow \Xi_{cc}\bar{K}$	-0.04	-1.89	-0.02	-0.04	-2.23	-0.02	-0.04	-2.73	-0.02
	$\Omega_{cc}\eta \rightarrow \Omega_{cc}\eta$	-0.03	-0.24	0.54	-0.03	-0.30	0.50	-0.03	-0.36	0.46
$(-1, 1)$	$\Omega_{cc}\pi \rightarrow \Omega_{cc}\pi$	0.0	0.0	0.0	0.0	0.0	0.0	0.0	0.0	0.0
	$\Xi_{cc}\bar{K} \rightarrow \Xi_{cc}\bar{K}$	0.0	0.0	0.0	0.0	0.0	0.0	0.0	0.0	0.0
$(0, \frac{1}{2})$	$\Xi_{cc}\pi \rightarrow \Xi_{cc}\pi$	-0.003	-8.85	-1.90	-0.003	-19.3	-1.51	-0.003	71.6	-1.25
	$\Xi_{cc}\eta \rightarrow \Xi_{cc}\eta$	-0.01	-0.06	0.14	-0.01	-0.07	0.12	-0.01	-0.09	0.12
	$\Omega_{cc}K \rightarrow \Omega_{cc}K$	-0.02	-0.55	-0.01	-0.02	-0.61	-0.01	-0.02	-0.68	-0.01

There are two unknown parameters: h_A and M . We need to assign appropriate values to them, so that scattering lengths can be evaluated numerically. Thanks to HQS, the LO coupling constant h_A can be related to the g in the Lagrangian (3.10) by $h_A = 2\sqrt{3}g$. The chiral limit mass M is replaced by the physical mass $M_{\psi'}$. The physical mass of spin-3/2 baryon is assumed to be $M_{\psi'} = m_{\psi} + \Delta$, where Δ is the mass splitting. Since the spin-1/2 and spin-3/2 baryons differ only in the relative orientation of the quark spins, the resultant difference in their masses is attributed to the spin-spin interaction in the viewpoint of

potential model. Here, following Ref. [67], we roughly take the difference to be around 100 MeV. Three values of Δ are adopted: $\Delta = 50$ MeV, $\Delta = 100$ MeV and $\Delta = 150$ MeV. Contributions of spin-3/2 baryons to the S - and P -wave scattering lengths are compiled in Table 12.

It can be seen from Table 12 that for S wave the size of the contribution of spin-3/2 baryons is nearly negligible. The s - and u -channel exchanges of ψ' , corresponding to diagram (a) and (b) in Figure 5 respectively, mainly affect the P -wave scattering lengths. For a given strong interaction, strangeness and isospin are conserved definitely. Therefore, the s -channel exchange of spin-3/2 Ξ'_{cc} and Ω'_{cc} states contribute only to the scattering processes with $(S, I) = (0, 1/2)$ and $(-1, 0)$, respectively. This can also be justified by seeing the coefficients $C_S^{(1)}$ in Table 1. Furthermore, we have checked that it dominates the a_{1+} scattering lengths in the two coupled channels with $(S, I) = (0, 1/2)$ and $(-1, 0)$, which is in accordance with the conservation law of total angular momentum. The remaining processes get contributions entirely from the crossed diagram, i.e. diagram (b) in Figure 5.

In parallel, one may also study the resonance contribution to the LECs with Eq. (5.12). In the viewpoint of effective field theory, a low-energy effective Lagrangian contains only low-lying degrees of freedom, while resonances at hard scale have been integrated out. The information of resonance contributions is regarded to be encoded in the LECs, i.e. the coefficients of the operators in the chiral effective Lagrangian without resonances. The pertinent contributions of resonances to the LECs can be efficiently achieved by a matching procedure carried out at the level of effective Lagrangian. Such a procedure has already been used, e.g., in the analyses of the LECs in pion-nucleon scattering [49, 104] and D - ϕ interactions [105]. In our current situation, we intend to utilize the above-mentioned technique to evaluate the influence of the ψ' states on the LECs. Specifically, the ψ' -exchange amplitudes in Eq. (5.12) are expanded in terms of $\nu = (s - u)/(4m)$, t and m_ϕ , and then compared to the contact-term contribution in Eqs. (3.16) and (3.18). As a result, the ψ' -exchange contributions to the $\mathcal{O}(p^2)$ LECs read

$$b_{1,2,4,6}^{\psi'} = 0, \quad b_3^{\psi'} = -\frac{h_A^2}{6\Delta}, \quad b_5^{\psi'} = -\frac{h_A^2 m^2}{48\Delta(m + \Delta)^2}, \quad b_7^{\psi'} = -\frac{h_A^2 m^2}{24\Delta}, \quad (5.14)$$

where m is the spin-1/2 baryon mass in the chiral limit. For the $\mathcal{O}(p^3)$ LECs, the ψ' states contribute as

$$c_{11}^{\psi'} = -\frac{h_A^2(2m^2 + 3m\Delta + 3\Delta^2)}{48\Delta^2(m + \Delta)^2}, \quad c_{12}^{\psi'} = -\frac{h_A^2 m^2}{96\Delta^2(m + \Delta)^2}, \quad (5.15)$$

$$c_{13}^{\psi'} = \frac{h_A^2 m}{96\Delta^2(m + \Delta)}, \quad c_{14}^{\psi'} = 0, \quad c_{20}^{\psi'} = \frac{h_A^2(3m + \Delta)}{48\Delta(m + \Delta)^2}. \quad (5.16)$$

For the sake of numerical estimation, we take the chiral limit mass m equal to the average of the physical masses of the Ξ_{cc} and Ω_{cc} , i.e., $m = (m_{\Xi_{cc}} + m_{\Omega_{cc}})/2 = 3679.8$ MeV. Numerical results, obtained with three different mass splitting values $\Delta = (50, 100, 150)$ MeV, are displayed in Table 13.

In Table 13, the magnitudes of the LECs become smaller as the mass splitting Δ gets larger, which can be inferred from Eqs. (5.14), (5.15) and (5.16). Consequently, the spin-3/2 baryon contribution to the scattering lengths is expected to decrease as Δ increases.

Table 13. Results of Born-term ψ' -exchange contributions to the LECs. Δ denotes the mass splitting between the spin-1/2 and spin-3/2 doubly charmed baryons.

NLO LECs	$\Delta = (50, 100, 150)$ MeV	NNLO LECs	$\Delta = (50, 100, 150)$ MeV
$b_1^{\psi'}$	0	$c_{11}^{\psi'}$	(-7.17, -1.78, -0.79)
$b_2^{\psi'}$	0	$c_{12}^{\psi'}$	(-1.76, -0.43, -0.19)
$b_3^{\psi'}$	(-1.44, -0.72, -0.48)	$c_{13}^{\psi'}$	(1.78, 0.44, 0.19)
$b_4^{\psi'}$	0	$c_{14}^{\psi'}$	0
$b_5^{\psi'}$	(-0.18, -0.09, -0.06)	$c_{20}^{\psi'}$	(0.14, 0.07, 0.05)
$b_6^{\psi'}$	0		
$b_7^{\psi'}$	(-4.89, -2.44, -1.63)		

In Table 12, such a behavior can be clearly observed e.g. for the P -wave scattering lengths a_{1-} . However, anomaly happens for the scattering lengths a_{1+} with $(S, I) = (-1, 0)$ and $(S, I) = (0, 1/2)$. This anomaly actually indicates that the spin-3/2 baryon fields can not be integrated out in the two channels. In other words, explicit inclusion of spin-3/2 doubly charmed baryons is necessary if one intends to well determine the P -wave scattering length with $J^P = (3/2)^+$ and $(S, I) \in \{(-1, 0), (0, 1/2)\}$.

5.4 S -wave Phase shifts

With the chiral amplitudes, one can compute partial-wave phase shifts straightforwardly, which are functions of the CM energy \sqrt{s} . Although it is undoable to extract phase shifts experimentally, they can be related to energy levels according to Lüscher formula [74] and its extensions [75–78], which can be computed by lattice simulations in future.

Usually, the partial-wave amplitude $f_{\ell\pm}^{(S,I)}(s)$ from BChPT do not obey partial wave unitarity exactly, since they are derived perturbatively up to a certain order. The method of extracting phase shifts from perturbative amplitudes has been discussed, e.g. in Ref. [103]. Namely, one can calculate the phase shifts in the elastic scattering region by using

$$\delta_{\ell\pm}^{(S,I)}(s) = \arctan \left\{ |\mathbf{q}| \operatorname{Re} \left[f_{\ell\pm}^{(S,I)}(s) \right] \right\}, \quad (5.17)$$

where $|\mathbf{q}|$ is the modulus of the CM momentum. In the present work, we are only interested in the S -wave interactions, whose strength is expected to be stronger than that of higher partial waves. Moreover, one is allowed to ignore the effects of the spin-3/2 HQS cousins of the spin-1/2 doubly charmed baryons, since their impact on the S -wave phase shifts are negligible, as discussed in the preceding subsection.

In Figure 6, the S -wave phase shifts for the processes of elastic scattering are plotted for the energy region from threshold $\sqrt{s_{\text{th}}}$ to the point $\sqrt{s_{\text{th}}} + 150$ MeV. The blue solid lines stand for our results up to the order of $\mathcal{O}(p^3)$. The light-blue bands corresponds to the uncertainties propagated from the errors of LECs via the method of Monte Carlo technique. In the figure, we also show the phase shifts order by order. The $\mathcal{O}(p)$, $\mathcal{O}(p^2)$ and $\mathcal{O}(p^3)$

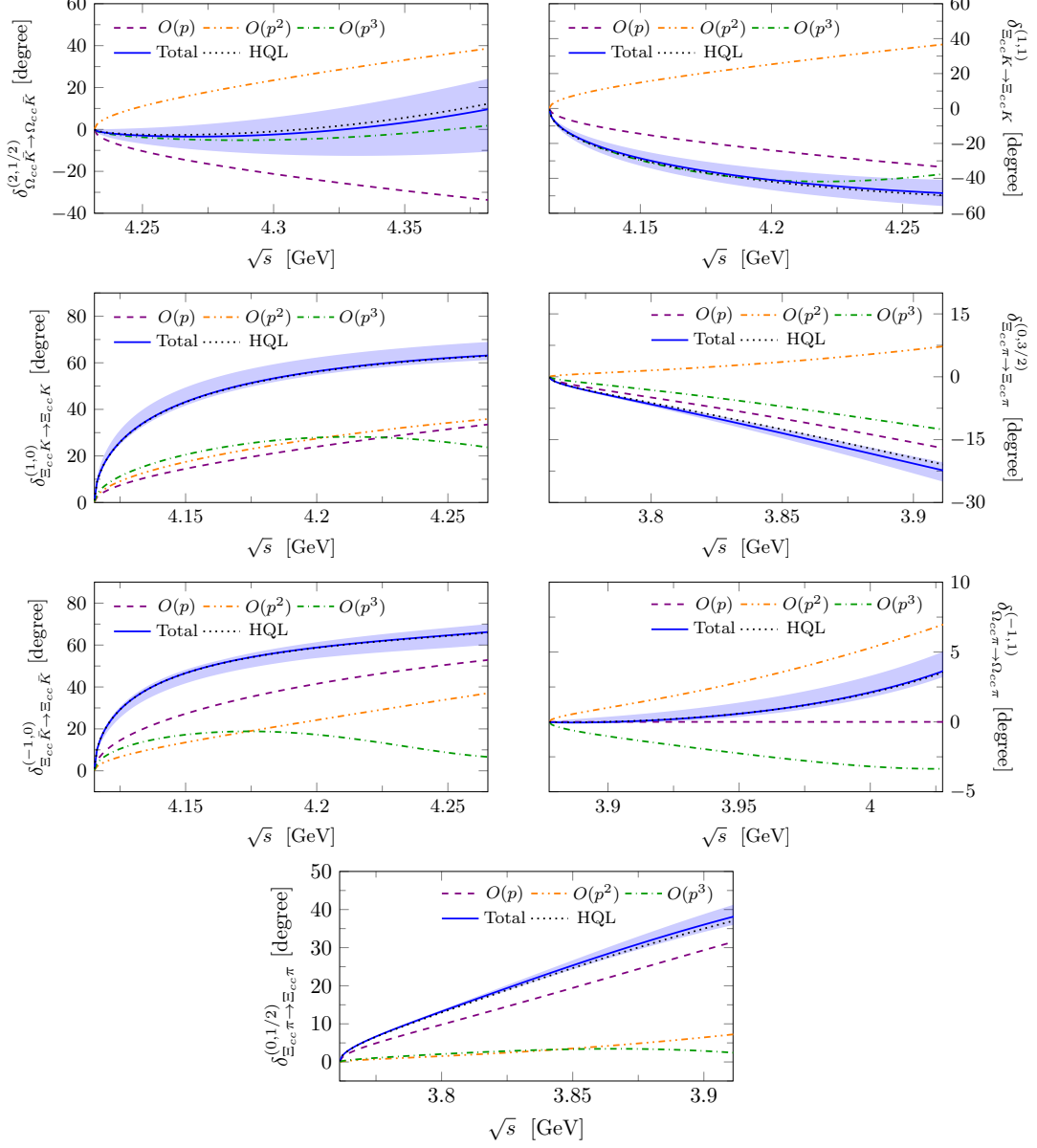


Figure 6. Results of S -wave phase shifts. The $\mathcal{O}(p)$, $\mathcal{O}(p^2)$ and $\mathcal{O}(p^3)$ contributions are represented by violet dashed, orange dash-dot-dotted, green dash-dotted lines, in order. The blue solid lines with bands stand for the total contribution. For comparison, the HQL results (black dotted lines) are also shown.

contributions are represented by violet dashed, orange dash-dot-dotted, green dash-dotted lines, in order. It can be seen that the convergence properties of the chiral expansion in the two elastic channels, $\Xi_{cc}\pi$ with $(S, I) = (0, 1/2)$ and $(0, 3/2)$ are relatively better, compared to the other channels. In fact, most of the LECs we used here are estimated by imposing HDA symmetry, while some of the LECs in the $\mathcal{O}(p^3)$ tree amplitudes are simply assumed to be zero under the requirement of naturalness. Therefore, a solid conclusion on the convergence properties can be drawn only when relevant lattice QCD data are available. For comparison, the HQL results of phase shifts are shown as well, which are obtained by setting $g = 0$. They are represented by the black dotted lines in the figure. It is found that the HQL-vanishing diagrams contribute slightly to the phase shifts, which is similar to the case of S -wave scattering lengths.

6 Summary and outlook

In this work, we have performed a NNLO calculation of the scattering amplitudes for the interactions between NGBs and doubly charmed baryons within the framework of relativistic BChPT. The EOMS scheme is employed to handle with the UV divergences and the PCB terms originating from the loops. We find that most of the unknown LECs in the chiral effective Lagrangians can be pinned down by making use of the HDA symmetry. The obtained LEC values enable us to make predictions of the S - and P -wave scattering lengths. We show that the HQL-surviving diagrams dominate the contribution to the S -wave scattering lengths, while the HQL-vanishing ones contribute marginally. The influence of spin-3/2 double-charm baryons on the scattering lengths is also evaluated in detail. Their contributions to the LECs are estimated as well. For future reference, the energy-dependent S -wave phase shifts are plotted for the elastic scattering channels in the energy regions near the lowest thresholds. Our chiral results can be applied to perform chiral extrapolations of future lattice QCD data, and can also be used to investigate the spectroscopy of doubly heavy baryons systematically.

A Γ -functions and β -functions

In this appendix, the Γ -functions in Eq. (4.24) and the UV- renormalization β -functions in Eq. (4.17) are listed. Their specific expressions read

$$\begin{aligned}\Gamma_4 &= \frac{1}{8}, \\ \Gamma_5 &= \frac{3}{8}, \\ \Gamma_6 &= \frac{11}{144}, \\ \Gamma_8 &= \frac{5}{48}, \\ \beta_m &= \frac{8g^2m^3}{3}, \\ \beta_g &= \frac{g(-9 + 2g^2)m^2}{3},\end{aligned}$$

$$\begin{aligned}
\beta_{b_1} &= -\frac{4g^2m}{9}, \\
\beta_{b_2} &= -\frac{5g^2m}{12}, \\
\beta_{b_3} &= -\frac{3(-1+2g^2+3g^4)m}{16}, \\
\beta_{b_4} &= \frac{(1-10g^2+5g^4)m}{16}, \\
\beta_{b_5} &= -\frac{3(-1+g^2)^2}{64m}, \\
\beta_{b_6} &= -\frac{(-1+g^2)^2}{32m}, \\
\beta_{b_7} &= \frac{3(-1-2g^2+3g^4)m}{32}, \\
\beta_{c_{11}} &= \frac{1-4g^2+3g^4}{64}, \\
\beta_{c_{12}} &= 0, \\
\beta_{c_{13}} &= -\frac{3(-1+g^2)^2}{128m}, \\
\beta_{c_{14}} &= -\frac{(-1+g^2)^2}{64m}, \\
\beta_{c_{15}} &= -\frac{3(g^3-g)}{32}, \\
\beta_{c_{16}} &= \frac{g(1-g^2)}{8}, \\
\beta_{c_{17}} &= -\frac{g-g^3}{16}, \\
\beta_{c_{18}} &= 0, \\
\beta_{c_{19}} &= 0, \\
\beta_{c_{20}} &= \frac{1-g^2}{32}.
\end{aligned} \tag{A.1}$$

B $\tilde{\beta}$ -functions

The $\tilde{\beta}$ -functions in Eq. (4.18) are given as follows.

$$\begin{aligned}
\tilde{\beta}_m &= -\frac{8g^2m}{3}A_0(m^2), \\
\tilde{\beta}_g &= \frac{2g^3m^2}{3} - \frac{g(-9+2g^2)}{3}A_0(m^2), \\
\tilde{\beta}_{b_1} &= \frac{4g^2m}{9} + \frac{4g^2}{9m}A_0(m^2), \\
\tilde{\beta}_{b_2} &= \frac{5g^2m}{12} + \frac{5g^2}{12m}A_0(m^2), \\
\tilde{\beta}_{b_3} &= \frac{g^2(g^2+3)m}{4} + \frac{3(3g^4+2g^2-1)}{16m}A_0(m^2),
\end{aligned}$$

$$\begin{aligned}
\tilde{\beta}_{b_4} &= \frac{g^2 (5g^2 - 1) m}{4} - \frac{5g^4 - 10g^2 + 1}{16m} A_0(m^2), \\
\tilde{\beta}_{b_5} &= \frac{5g^4 + 9}{96m} + \frac{3(g^2 - 1)^2}{64m^3} A_0(m^2), \\
\tilde{\beta}_{b_6} &= \frac{g^4 + 1}{16m} + \frac{(g^2 - 1)^2}{32m^3} A_0(m^2), \\
\tilde{\beta}_{b_7} &= -\frac{g^2 (3g^2 + 5) m}{12} - \frac{3(3g^4 - 2g^2 - 1)}{32m} A_0(m^2), \tag{B.1}
\end{aligned}$$

where A_0 is defined in Appendix C.

C Loop corrections to the baryon masses and wave function renormalization constants

In our calculation, the N -point ($N \leq 4$) one-loop scalar integrals [106] are defined by

$$T^N = \frac{(2\pi\mu)^{4-d}}{i\pi^2} \int \frac{d^d k}{[k^2 - m_0^2 + i\epsilon] [(k + p_1)^2 - m_1^2 + i\epsilon] \cdots [(k + p_{N-1})^2 - m_{N-1}^2 + i\epsilon]},$$

with ϵ being an infinitesimal positive number. Traditionally, the one-, two-, three- and four-point one-loop scalar integrals are denoted by A_0 , B_0 , C_0 and D_0 , in order. To be specific, one has

$$T^1 = A_0(m_0^2), \tag{C.1}$$

$$T^2 = B_0(p_1^2, m_0^2, m_1^2), \tag{C.2}$$

$$T^3 = C_0(p_1^2, (p_2 - p_1)^2, p_2^2, m_0^2, m_1^2, m_2^2), \tag{C.3}$$

$$T^4 = D_0(p_1^2, (p_2 - p_1)^2, (p_3 - p_2)^2, p_3^2, p_2^2, (p_3 - p_1)^2, m_0^2, m_1^2, m_2^2, m_3^2). \tag{C.4}$$

With these definitions, the chiral corrections concerning the baryon masses and wave function renormalization constants are clearly shown in what follows. The one-loop corrections to the Ξ_{cc} and Ω_{cc} baryons read

$$\begin{aligned}
\delta m_{\Xi_{cc}}^{\text{loop}} &= \frac{g^2}{12m_{\Xi_{cc}} F^2} \left\{ 3(m_{\Xi_{cc}}^2 - m_{\Omega_{cc}}^2) A_0(m_K^2) + 3(m_{\Xi_{cc}} + m_{\Omega_{cc}})^2 A_0(m_{\Omega_{cc}}^2) \right. \\
&\quad + 20m_{\Xi_{cc}}^2 A_0(m_{\Xi_{cc}}^2) + 2m_\eta^2 m_{\Xi_{cc}}^2 B_0(m_{\Xi_{cc}}^2, m_\eta^2, m_{\Xi_{cc}}^2) \\
&\quad - 3[(m_{\Omega_{cc}} - m_{\Xi_{cc}})^2 - m_K^2] (m_{\Omega_{cc}} + m_{\Xi_{cc}})^2 B_0(m_{\Xi_{cc}}^2, m_K^2, m_{\Omega_{cc}}^2) \\
&\quad \left. + 18m_\pi^2 m_{\Xi_{cc}}^2 B_0(m_{\Xi_{cc}}^2, m_\pi^2, m_{\Xi_{cc}}^2) \right\}, \\
\delta m_{\Omega_{cc}}^{\text{loop}} &= \frac{g^2}{6m_{\Omega_{cc}} F^2} \left\{ 3(m_{\Omega_{cc}}^2 - m_{\Xi_{cc}}^2) A_0(m_K^2) + 4m_{\Omega_{cc}}^2 A_0(m_{\Omega_{cc}}^2) \right. \\
&\quad + 3(m_{\Omega_{cc}} + m_{\Xi_{cc}})^2 A_0(m_{\Xi_{cc}}^2) + 4m_\eta^2 m_{\Omega_{cc}}^2 B_0(m_{\Omega_{cc}}^2, m_\eta^2, m_{\Omega_{cc}}^2) \\
&\quad \left. - 3[(m_{\Omega_{cc}} - m_{\Xi_{cc}})^2 - m_K^2] (m_{\Omega_{cc}} + m_{\Xi_{cc}})^2 B_0(m_{\Omega_{cc}}^2, m_K^2, m_{\Xi_{cc}}^2) \right\}. \tag{C.5}
\end{aligned}$$

For the Ξ_{cc}^{++} and Ξ_{cc}^+ states, the wave function renormalization constants are defined by

$$\mathcal{Z}_{\Xi_{cc}} = 1 + \delta\mathcal{Z}_{\Xi_{cc}} , \quad (\text{C.6})$$

with

$$\begin{aligned} \delta\mathcal{Z}_{\Xi_{cc}} = & \frac{g^2}{12F^2} \left\{ \frac{1}{m_\eta^2 - 4m_{\Xi_{cc}}^2} [(2d-3)m_\eta^2 - 4(d-1)m_{\Xi_{cc}}^2] A_0(m_\eta^2) \right. \\ & + \frac{3}{m_{\Xi_{cc}}^2 \Delta_{\psi K}^2} \{ (d-1)(m_{\Omega_{cc}} + m_{\Xi_{cc}})^2 (m_{\Omega_{cc}}^2 + m_{\Xi_{cc}}^2 - m_K^2) + 2m_K^2 m_{\Omega_{cc}} m_{\Xi_{cc}} \} A_0(m_K^2) \\ & - \frac{3(m_{\Omega_{cc}} + m_{\Xi_{cc}})}{m_{\Xi_{cc}}^2 \Delta_{\psi K}^2} \{ (d-1)(m_{\Omega_{cc}} + m_{\Xi_{cc}})(m_{\Omega_{cc}}^2 - m_{\Xi_{cc}}^2 - m_K^2) + 2m_K^2 m_{\Xi_{cc}} \} A_0(m_{\Omega_{cc}}^2) \\ & + \frac{9}{m_\pi^2 - 4m_{\Xi_{cc}}^2} [(2d-3)m_\pi^2 - 4(d-1)m_{\Xi_{cc}}^2] A_0(m_\pi^2) \\ & + \frac{4(d-2)}{(m_\eta^2 - 4m_{\Xi_{cc}}^2)(m_\pi^2 - 4m_{\Xi_{cc}}^2)} [18m_\pi^2 m_{\Xi_{cc}}^2 - m_\eta^2(5m_\pi^2 - 2m_{\Xi_{cc}}^2)] A_0(m_{\Xi_{cc}}^2) \\ & - \frac{2m_\eta^2}{m_\eta^2 - 4m_{\Xi_{cc}}^2} [(d-2)m_\eta^2 - 2(d-1)m_{\Xi_{cc}}^2] B_0(m_{\Xi_{cc}}^2, m_\eta^2, m_{\Xi_{cc}}^2) \\ & + \frac{3(m_{\Omega_{cc}} + m_{\Xi_{cc}})}{m_{\Xi_{cc}}^2 \Delta_{\psi K}^2} \{ (d-1)(m_{\Omega_{cc}} + m_{\Xi_{cc}})(m_{\Omega_{cc}}^4 - m_{\Xi_{cc}}^4 + m_K^4 - 2m_K^2 m_{\Omega_{cc}}^2) \\ & + 2m_K^2 m_{\Xi_{cc}} [(m_{\Omega_{cc}} - m_{\Xi_{cc}})^2 - m_K^2] \} B_0(m_{\Xi_{cc}}^2, m_K^2, m_{\Omega_{cc}}^2) \\ & \left. - \frac{18m_\pi^2}{(m_\pi^2 - 4m_{\Xi_{cc}}^2)} \{ (d-2)m_\pi^2 - 2(d-1)m_{\Xi_{cc}}^2 \} B_0(m_{\Xi_{cc}}^2, m_\pi^2, m_{\Xi_{cc}}^2) \right\} , \quad (\text{C.7}) \end{aligned}$$

and

$$\begin{aligned} \delta\mathcal{Z}_{\Omega_{cc}} = & \frac{g^2}{6F^2} \left\{ \frac{2}{m_\eta^2 - 4m_{\Omega_{cc}}^2} \{ [(2d-3)m_\eta^2 - 4(d-1)m_{\Omega_{cc}}^2] \} A_0(m_\eta^2) - \frac{4(d-2)m_\eta^2}{m_\eta^2 - 4m_{\Omega_{cc}}^2} A_0(m_{\Omega_{cc}}^2) \right. \\ & + \frac{3}{m_{\Omega_{cc}}^2 \Delta_{\psi K}^2} \{ (d-1)(m_{\Omega_{cc}} + m_{\Xi_{cc}})^2 (m_{\Omega_{cc}}^2 + m_{\Xi_{cc}}^2 - m_K^2) + 2m_K^2 m_{\Omega_{cc}} m_{\Xi_{cc}} \} A_0(m_K^2) \\ & + \frac{3(m_{\Omega_{cc}} + m_{\Xi_{cc}})}{m_{\Omega_{cc}}^2 \Delta_{\psi K}^2} \{ (d-1)(m_{\Omega_{cc}} + m_{\Xi_{cc}})(m_{\Omega_{cc}}^2 - m_{\Xi_{cc}}^2 + m_K^2) - 2m_K^2 m_{\Omega_{cc}} \} A_0(m_{\Xi_{cc}}^2) \\ & - \frac{4m_\eta^2}{m_\eta^2 - 4m_{\Omega_{cc}}^2} [(d-2)m_\eta^2 - 2(d-1)m_{\Omega_{cc}}^2] B_0(m_{\Omega_{cc}}^2, m_\eta^2, m_{\Omega_{cc}}^2) \\ & + \frac{3(m_{\Omega_{cc}} + m_{\Xi_{cc}})}{m_{\Omega_{cc}}^2 \Delta_{\psi K}^2} \{ (d-1)(m_{\Xi_{cc}} + m_{\Omega_{cc}})(m_K^4 - (m_{\Omega_{cc}}^4 - m_{\Xi_{cc}}^4) - 2m_K^2 m_{\Xi_{cc}}^2) \\ & + 2m_K^2 m_{\Omega_{cc}} [(m_{\Xi_{cc}} - m_{\Omega_{cc}})^2 - m_K^2] \} B_0(m_{\Omega_{cc}}^2, m_K^2, m_{\Xi_{cc}}^2) \left. \right\} , \quad (\text{C.8}) \end{aligned}$$

where the abbreviation $\Delta_{\psi K}^2 \equiv [(m_{\Omega_{cc}} + m_{\Xi_{cc}})^2 - m_K^2]$ has been used.

D Heavy diquark-antiquark symmetry

In HQL, charmed mesons and doubly charmed baryons can form a super multiplet according to the HDA symmetry. A uniform Lagrangian can be constructed with common

LECs. Following Refs. [67, 107–109], we define a super field \mathcal{S} in the form as

$$\mathcal{S} \equiv \begin{pmatrix} \tilde{H} & 0 \\ 0 & T \end{pmatrix}, \quad \bar{\mathcal{S}} \equiv \begin{pmatrix} \tilde{H} & 0 \\ 0 & \bar{T} \end{pmatrix}, \quad (\text{D.1})$$

which comprises both the charmed mesons and doubly charmed baryons. The pseudoscalar and vector charmed mesons are collected in the \tilde{H} and \bar{H} fields as

$$\begin{aligned} \tilde{H} &= \sqrt{\bar{m}_D}(\tilde{P}^* + i\tilde{P}\gamma_5)\frac{1-\psi}{2}, & \bar{H} &= \frac{1-\psi}{2}\sqrt{\bar{m}_D}(\tilde{P}^{*\dagger} + i\tilde{P}^\dagger\gamma_5), \\ \tilde{P} &= (\bar{D}^0, D^-, D_s^-), & \tilde{P}_\mu^* &= (\bar{D}^{*0}, D^{*-}, D_s^{*-})_\mu, \end{aligned}$$

where \bar{m}_D is the charmed meson mass in the HQL. Likewise, the spin-1/2 and spin-3/2 doubly charmed baryons are contained in T^μ and \bar{T}^μ fields as

$$\begin{aligned} T^\mu &= \psi'^\mu + \sqrt{\frac{1}{3}}(\gamma^\mu + v^\mu)\gamma^5\psi, & \bar{T}^\mu &= \bar{\psi}'^\mu - \sqrt{\frac{1}{3}}\bar{\psi}\gamma^5(\gamma^\mu + v^\mu), \\ \psi &= (\Xi_{cc}^{++}, \Xi_{cc}^+, \Omega_{cc}^+)^T, & \psi'_\mu &= (\Xi_{cc}'^{++}, \Xi_{cc}'^+, \Omega_{cc}'^+)_\mu^T. \end{aligned} \quad (\text{D.2})$$

Accordingly, auxiliary chiral blocks for the NGBs should be introduced. We need

$$\begin{aligned} \hat{\chi}_\pm &= E_2 \otimes \chi_\pm = \begin{pmatrix} \chi_\pm & 0 \\ 0 & \chi_\pm \end{pmatrix}, & \hat{\tilde{\chi}}_\pm &= E_2 \otimes \tilde{\chi}_\pm, \\ \hat{u} &= E_2 \otimes u, & \hat{D} &= E_2 \otimes D, & \hat{h} &= E_2 \otimes h, \end{aligned} \quad (\text{D.3})$$

with E_2 the two-dimensional identity matrix. With the superfield \mathcal{S} and the super chiral blocks, chiral effective Lagrangians in HQL up to $\mathcal{O}(p^3)$ can be constructed straightforwardly, which read

$$\begin{aligned} \mathcal{L}_{\mathcal{S}\phi}^{(1)} &= i\text{Tr}(\mathcal{S}v \cdot D\bar{\mathcal{S}}) - \frac{g_h}{2}\text{Tr}(\mathcal{S}\hat{u}^\mu\gamma_\mu\gamma_5\bar{\mathcal{S}}), \\ \mathcal{L}_{\mathcal{S}\phi}^{(2)} &= d_1\text{Tr}(\mathcal{S}\bar{\mathcal{S}})\langle\chi_+\rangle + d_2\text{Tr}(\mathcal{S}\hat{\chi}_+\bar{\mathcal{S}}) - d_3\text{Tr}(\mathcal{S}\bar{\mathcal{S}})\langle(v \cdot u)^2\rangle - d_4\text{Tr}(\mathcal{S}(v \cdot \hat{u})^2\bar{\mathcal{S}}) \\ &\quad - d_5\text{Tr}(\mathcal{S}\bar{\mathcal{S}})\langle u^2\rangle - d_6\text{Tr}(\mathcal{S}\hat{u}^2\bar{\mathcal{S}}) - id_7\text{Tr}(\mathcal{S}[\hat{u}^\mu, \hat{u}^\nu]\sigma_{\mu\nu}\bar{\mathcal{S}}), \\ \mathcal{L}_{\mathcal{S}\phi}^{(3)} &= ie_1\text{Tr}(\mathcal{S}[\hat{u}_\mu, \hat{h}^{\mu\nu}]v_\nu\bar{\mathcal{S}}) + ie_2\text{Tr}(\mathcal{S}[v \cdot \hat{u}, \hat{h}^{\mu\nu}]v_\mu v_\nu\bar{\mathcal{S}}) + e_3\text{Tr}(\mathcal{S}\{\hat{u}^\mu, \hat{h}^{\nu\rho}\}\sigma_{\mu\nu}v_\rho\bar{\mathcal{S}}) \\ &\quad + e_4\text{Tr}(\mathcal{S}\sigma_{\mu\nu}\langle u^\mu h^{\nu\rho}\rangle v_\rho\bar{\mathcal{S}}) + e_5\text{Tr}(\mathcal{S}\{\hat{u}^\nu, \hat{\chi}_+\}\gamma_5\gamma_\nu\bar{\mathcal{S}}) + e_6\text{Tr}(\mathcal{S}\hat{u}^\mu\gamma_5\gamma_\mu\langle\chi_+\rangle\bar{\mathcal{S}}) \\ &\quad + e_7\text{Tr}(\mathcal{S}\gamma_5\gamma_\mu\langle u^\mu\tilde{\chi}_+\rangle\bar{\mathcal{S}}) + ie_8\text{Tr}(\mathcal{S}\gamma_5\gamma_\nu[\hat{D}^\nu, \hat{\chi}_-]\bar{\mathcal{S}}) + ie_9\text{Tr}(\mathcal{S}\gamma_5\gamma_\nu\langle[D^\nu, \chi_-]\rangle\bar{\mathcal{S}}) \\ &\quad + e_{10}(\text{Tr}(\mathcal{S}[\hat{\chi}_-, v \cdot \hat{u}]\bar{\mathcal{S}})). \end{aligned} \quad (\text{D.4})$$

Here, d_i ($i = 1, 2, \dots, 7$) and e_i ($i = 1, 2, \dots, 10$) are LECs common to $D\phi$, $D^*\phi$, $\psi\phi$ and $\psi'\phi$ interactions. The symbol $\text{Tr}(\dots)$ denotes the trace in the Dirac space, and v_μ is the baryon four-velocity satisfying $v^2 = 1$.

On the other hand, relativistic $D\phi$ Lagrangians can be found in Ref. [72], which are

$$\mathcal{L}_{P\phi}^{(1)} = D_\mu P D^\mu P^\dagger - m_P^2 P P^\dagger + ig_0(P_\mu^* u^\mu P^\dagger - P u^\mu P_\mu^*), \quad (\text{D.5})$$

$$\begin{aligned} \mathcal{L}_{P\phi}^{(2)} = & -h_0 P \langle \chi_+ \rangle P^\dagger - h_1 P \chi_+ P^\dagger + h_2 P \langle u^2 \rangle P^\dagger - h_3 P u^2 P^\dagger + h_4 D_\mu P \langle u^\mu u^\nu \rangle D_\nu P^\dagger \\ & - h_5 D_\mu P \{u^\mu, u^\nu\} D_\nu P^\dagger , \end{aligned} \quad (\text{D.6})$$

$$\mathcal{L}_{P\phi}^{(3)} = i g_1 P [\chi_-, u^\mu] D_\mu P^\dagger + g_2 P [u_\mu, h^{\mu\nu}] D_\nu P^\dagger + \frac{g_3}{2} P [u^\mu, h^{\nu\rho}] \{D_\mu, \{D_\nu, D_\rho\}\} P^\dagger . \quad (\text{D.7})$$

Here h_i ($i = 0, 1, \dots, 5$) and g_i ($i = 1, 2, 3$) are LECs, whose values have already been determined in Ref. [72].

Our aim is to derive relations between the $\psi\phi$ LECs in the Lagrangians (3.10), (3.11) and (3.12) and the $D\phi$ LECs in Lagrangians (D.5), (D.6) and (D.7). This can be established in three steps. First, one performs non-relativistic projection of the relativistic $D\phi$ Lagrangians to get their HQL counterparts. By comparing with the HQL Lagrangians in Eq. (D.4), one finds

$$\begin{aligned} g_0 = g_h \bar{m}_D, \quad h_0 = 2d_1 \bar{m}_D, \quad h_1 = 2d_2 \bar{m}_D, \quad h_2 = 2d_5 \bar{m}_D, \quad h_3 = -2d_6 \bar{m}_D, \\ h_4 = \frac{2d_3}{\bar{m}_D}, \quad h_5 = -\frac{d_4}{\bar{m}_D}; \quad g_1 = 2e_{10}, \quad g_2 = -2e_1, \quad g_3 = \frac{e_2}{\bar{m}_D^2} . \end{aligned} \quad (\text{D.8})$$

Second, one repeats the same procedure for the relativistic $\psi\phi$ Lagrangians and gets

$$\begin{aligned} g = -\frac{1}{3}g_h, \quad b_1 = -(d_1 + \frac{1}{3}d_2), \quad b_2 = -d_2, \quad b_3 = d_6, \quad b_4 = d_5, \\ b_5 = -\frac{d_4}{8}, \quad b_6 = -\frac{d_3}{4}, \quad b_7 = -\frac{d_7}{3}; \quad c_{11} = -e_1, \quad c_{12} = \frac{e_2}{4}, \\ c_{13} = \frac{e_3}{6}, \quad c_{14} = \frac{e_4}{6}, \quad c_{15} = \frac{e_5}{3}, \quad c_{16} = \frac{e_6}{3}, \quad c_{17} = \frac{e_7}{3}, \\ c_{18} = \frac{e_8}{3}, \quad c_{19} = \frac{e_9}{3}, \quad c_{20} = -e_{10}. \end{aligned} \quad (\text{D.9})$$

Eventually, the identities in Eq. (D.8) and Eq. (D.9) lead to the following relations between the relativistic $\psi\phi$ and $D\phi$ LECs:

$$\begin{aligned} g = -\frac{1}{3\bar{m}_D}g_0, \quad b_1 = -\frac{1}{2\bar{m}_D}(h_0 + \frac{1}{3}h_1), \quad b_2 = -\frac{1}{2\bar{m}_D}h_1, \\ b_3 = -\frac{1}{2\bar{m}_D}h_3, \quad b_4 = \frac{1}{2\bar{m}_D}h_2, \quad b_5 = \frac{\bar{m}_D}{8}h_5, \\ b_6 = -\frac{\bar{m}_D}{8}h_4, \quad c_{11} = \frac{g_2}{2}, \quad c_{12} = \frac{\bar{m}_D^2}{4}g_3, \quad c_{20} = -\frac{g_1}{2} . \end{aligned} \quad (\text{D.10})$$

Acknowledgments

We would like to thank Shao-Zhou Jiang and Zhan-Wei Liu for helpful discussions. This work is supported by National Nature Science Foundations of China (NSFC) under Contract Nos. 12275076, 11905258 and by the Fundamental Research Funds for the Central Universities under Contract No. 531118010379.

References

- [1] E. Klempt and J. M. Richard, Baryon spectroscopy, Rev. Mod. Phys. **82** (2010), 1095-1153.

- [2] H. X. Chen, W. Chen, X. Liu, Y. R. Liu and S. L. Zhu, A review of the open charm and open bottom systems, Rept. Prog. Phys. **80** (2017) no.7, 076201.
- [3] F. K. Guo, C. Hanhart, U. G. Meißner, Q. Wang, Q. Zhao and B. S. Zou, Hadronic molecules, Rev. Mod. Phys. **90** (2018) no.1, 015004 [erratum: Rev. Mod. Phys. **94** (2022) no.2, 029901].
- [4] S. Chen, Y. Li, W. Qian, Z. Shen, Y. Xie, Z. Yang, L. Zhang and Y. Zhang, Heavy Flavour Physics and CP Violation at LHCb: a Ten-Year Review, [arXiv:2111.14360 [hep-ex]].
- [5] H. X. Chen, W. Chen, X. Liu, Y. R. Liu and S. L. Zhu, An updated review of the new hadron states, Rept. Prog. Phys. **86** (2023) no.2, 026201.
- [6] L. Meng, B. Wang, G. J. Wang and S. L. Zhu, Chiral perturbation theory for heavy hadrons and chiral effective field theory for heavy hadronic molecules, [arXiv:2204.08716 [hep-ph]].
- [7] M. Gell-Mann, A Schematic Model of Baryons and Mesons, Phys. Lett. **8** (1964), 214-215.
- [8] G. T. Bodwin, E. Braaten and G. P. Lepage, Rigorous QCD analysis of inclusive annihilation and production of heavy quarkonium, Phys. Rev. D **51** (1995), 1125-1171 [erratum: Phys. Rev. D **55** (1997), 5853].
- [9] M. Mattson *et al.* [SELEX], First Observation of the Doubly Charmed Baryon Ξ_{cc}^+ , Phys. Rev. Lett. **89** (2002), 112001.
- [10] A. Ocherashvili *et al.* [SELEX], Confirmation of the double charm baryon $\Xi^+(cc)(3520)$ via its decay to pD^+K^- , Phys. Lett. B **628** (2005), 18-24.
- [11] R. Aaij *et al.* [LHCb], Observation of the doubly charmed baryon Ξ_{cc}^{++} , Phys. Rev. Lett. **119** (2017) no.11, 112001.
- [12] R. Aaij *et al.* [LHCb], First Observation of the Doubly Charmed Baryon Decay $\Xi_{cc}^{++} \rightarrow \Xi_c^+ \pi^+$, Phys. Rev. Lett. **121** (2018) no.16, 162002.
- [13] F. S. Yu, H. Y. Jiang, R. H. Li, C. D. Lü, W. Wang and Z. X. Zhao, Discovery Potentials of Doubly Charmed Baryons, Chin. Phys. C **42** (2018) no.5, 051001.
- [14] R. Aaij *et al.* [LHCb], Measurement of the Lifetime of the Doubly Charmed Baryon Ξ_{cc}^{++} , Phys. Rev. Lett. **121** (2018) no.5, 052002.
- [15] R. Aaij *et al.* [LHCb], Precision measurement of the Ξ_{cc}^{++} mass, JHEP **02** (2020), 049.
- [16] R. Aaij *et al.* [LHCb], Measurement of Ξ_{cc}^{++} production in pp collisions at $\sqrt{s} = 13$ TeV, Chin. Phys. C **44** (2020) no.2, 022001.
- [17] R. Aaij *et al.* [LHCb], Search for the doubly charmed baryon Ξ_{cc}^+ , Sci. China Phys. Mech. Astron. **63** (2020) no.2, 221062.
- [18] R. Aaij *et al.* [LHCb], Search for the doubly charmed baryon Ξ_{cc}^+ in the $\Xi_c^+ \pi^- \pi^+$ final state, JHEP **12** (2021), 107.
- [19] R. Aaij *et al.* [LHCb], Search for the doubly charmed baryon Ω_{cc}^+ , Sci. China Phys. Mech. Astron. **64** (2021) no.10, 101062.
- [20] S. P. Ratti, New results on c-baryons and a search for cc-baryons in FOCUS, Nucl. Phys. B Proc. Suppl. **115** (2003), 33-36.
- [21] B. Aubert *et al.* [BaBar], Search for doubly charmed baryons Ξ_{cc}^+ and Ξ_{cc}^{++} in BABAR, Phys. Rev. D **74** (2006), 011103.

- [22] R. Chistov *et al.* [Belle], Observation of new states decaying into $\Lambda_c^+ K^- \pi^+$ and $\Lambda_c^+ K_S^0 \pi^-$, Phys. Rev. Lett. **97** (2006), 162001.
- [23] D. Ebert, R. N. Faustov, V. O. Galkin and A. P. Martynenko, Mass spectra of doubly heavy baryons in the relativistic quark model, Phys. Rev. D **66** (2002), 014008.
- [24] M. Karliner and J. L. Rosner, Baryons with two heavy quarks: Masses, production, decays, and detection, Phys. Rev. D **90** (2014) no.9, 094007.
- [25] J. G. Korner, M. Kramer and D. Pirjol, Heavy baryons, Prog. Part. Nucl. Phys. **33** (1994), 787-868.
- [26] R. Lewis, N. Mathur and R. M. Woloshyn, Charmed baryons in lattice QCD, Phys. Rev. D **64** (2001), 094509.
- [27] L. Liu, H. W. Lin, K. Orginos and A. Walker-Loud, Singly and Doubly Charmed $J = 1/2$ Baryon Spectrum from Lattice QCD, Phys. Rev. D **81** (2010), 094505.
- [28] Z. S. Brown, W. Detmold, S. Meinel and K. Orginos, Charmed bottom baryon spectroscopy from lattice QCD, Phys. Rev. D **90** (2014) no.9, 094507.
- [29] D. L. Yao, L. Y. Dai, H. Q. Zheng and Z. Y. Zhou, A review on partial-wave dynamics with chiral effective field theory and dispersion relation, Rept. Prog. Phys. **84** (2021) no.7, 076201.
- [30] A. Cerri, V. V. Gligorov, S. Malvezzi, J. Martin Camalich, J. Zupan, S. Akar, J. Alimena, B. C. Allanach, W. Altmannshofer and L. Anderlini, *et al.* Report from Working Group 4: Opportunities in Flavour Physics at the HL-LHC and HE-LHC, CERN Yellow Rep. Monogr. **7** (2019), 867-1158.
- [31] Q. F. Lü, K. L. Wang, L. Y. Xiao and X. H. Zhong, Mass spectra and radiative transitions of doubly heavy baryons in a relativized quark model, Phys. Rev. D **96** (2017) no.11, 114006.
- [32] W. Wang, F. S. Yu and Z. X. Zhao, Weak decays of doubly heavy baryons: the $1/2 \rightarrow 1/2$ case, Eur. Phys. J. C **77** (2017) no.11, 781.
- [33] H. W. Ke, F. Lu, X. H. Liu and X. Q. Li, Study on $\Xi_{cc} \rightarrow \Xi_c$ and $\Xi_{cc} \rightarrow \Xi'_c$ weak decays in the light-front quark model, Eur. Phys. J. C **80** (2020) no.2, 140.
- [34] H. W. Ke and X. Q. Li, Revisiting the transition $\Xi_{cc}^{++} \rightarrow \Xi_c^{'+}$ to understand the data from LHCb, Phys. Rev. D **105** (2022) no.9, 9.
- [35] X. Z. Weng, X. L. Chen and W. Z. Deng, Masses of doubly heavy-quark baryons in an extended chromomagnetic model, Phys. Rev. D **97** (2018) no.5, 054008.
- [36] W. Wang, Z. P. Xing and J. Xu, Weak Decays of Doubly Heavy Baryons: SU(3) Analysis, Eur. Phys. J. C **77** (2017) no.11, 800.
- [37] C. Q. Geng, Y. K. Hsiao, C. W. Liu and T. H. Tsai, Charmed Baryon Weak Decays with SU(3) Flavor Symmetry, JHEP **11** (2017), 147.
- [38] A. V. Berezhnoy, A. K. Likhoded and A. V. Luchinsky, Doubly heavy baryons at the LHC, Phys. Rev. D **98** (2018) no.11, 113004.
- [39] H. X. Chen, Q. Mao, W. Chen, X. Liu and S. L. Zhu, Establishing low-lying doubly charmed baryons, Phys. Rev. D **96** (2017) no.3, 031501 [erratum: Phys. Rev. D **96** (2017) no.11, 119902].
- [40] C. Y. Wang, C. Meng, Y. Q. Ma and K. T. Chao, NLO effects for doubly heavy baryons in QCD sum rules, Phys. Rev. D **99** (2019) no.1, 014018.

- [41] Z. G. Wang, Analysis of the doubly heavy baryon states and pentaquark states with QCD sum rules, *Eur. Phys. J. C* **78** (2018) no.10, 826.
- [42] Y. J. Shi, W. Wang and Z. X. Zhao, QCD Sum Rules Analysis of Weak Decays of Doubly-Heavy Baryons, *Eur. Phys. J. C* **80** (2020) no.6, 568.
- [43] N. Mathur and M. Padmanath, Lattice QCD study of doubly-charmed strange baryons, *Phys. Rev. D* **99** (2019) no.3, 031501.
- [44] H. Bahtiyar, K. U. Can, G. Erkol, P. Gubler, M. Oka and T. T. Takahashi, Charmed baryon spectrum from lattice QCD near the physical point, *Phys. Rev. D* **102** (2020) no.5, 054513.
- [45] M. J. Savage and M. B. Wise, Spectrum of baryons with two heavy quarks, *Phys. Lett. B* **248** (1990), 177-180.
- [46] S. Weinberg, Phenomenological Lagrangians, *Physica A* **96** (1979) no.1-2, 327-340.
- [47] J. Gasser and H. Leutwyler, Chiral Perturbation Theory to One Loop, *Annals Phys.* **158** (1984), 142.
- [48] J. Gasser and H. Leutwyler, Chiral Perturbation Theory: Expansions in the Mass of the Strange Quark, *Nucl. Phys. B* **250** (1985), 465-516.
- [49] V. Bernard, N. Kaiser and U. G. Meissner, Aspects of chiral pion - nucleon physics, *Nucl. Phys. A* **615** (1997), 483-500.
- [50] V. Bernard, Chiral Perturbation Theory and Baryon Properties, *Prog. Part. Nucl. Phys.* **60** (2008), 82-160.
- [51] Stefan Scherer and Matthias R. Schindler, *A Primer for Chiral Perturbation Theory*, Springer-Verlag Berlin Heidelberg, 2012.
- [52] J. Gasser, M. E. Sainio and A. Svarc, Nucleons with Chiral Loops, *Nucl. Phys. B* **307** (1988), 779-853.
- [53] E. E. Jenkins and A. V. Manohar, Baryon chiral perturbation theory using a heavy fermion Lagrangian, *Phys. Lett. B* **255** (1991), 558-562.
- [54] T. Becher and H. Leutwyler, Baryon chiral perturbation theory in manifestly Lorentz invariant form, *Eur. Phys. J. C* **9** (1999), 643-671.
- [55] T. Fuchs, J. Gegelia, G. Japaridze and S. Scherer, Renormalization of relativistic baryon chiral perturbation theory and power counting, *Phys. Rev. D* **68** (2003), 056005.
- [56] L. Geng, Recent developments in SU(3) covariant baryon chiral perturbation theory, *Front. Phys. (Beijing)* **8** (2013), 328-348.
- [57] S. J. Brodsky, F. K. Guo, C. Hanhart and U. G. Meissner, Isospin splittings of doubly heavy baryons, *Phys. Lett. B* **698** (2011), 251-255.
- [58] Z. F. Sun, Z. W. Liu, X. Liu and S. L. Zhu, Masses and axial currents of the doubly charmed baryons, *Phys. Rev. D* **91** (2015) no.9, 094030.
- [59] Z. F. Sun and M. J. Vicente Vacas, Masses of doubly charmed baryons in the extended on-mass-shell renormalization scheme, *Phys. Rev. D* **93** (2016) no.9, 094002.
- [60] H. S. Li, L. Meng, Z. W. Liu and S. L. Zhu, Radiative decays of the doubly charmed baryons in chiral perturbation theory, *Phys. Lett. B* **777** (2018), 169-176.
- [61] H. S. Li, L. Meng, Z. W. Liu and S. L. Zhu, Magnetic moments of the doubly charmed and bottom baryons, *Phys. Rev. D* **96** (2017) no.7, 076011.

- [62] A. N. Hiller Blin, Z. F. Sun and M. J. Vicente Vacas, Electromagnetic form factors of spin 1/2 doubly charmed baryons, *Phys. Rev. D* **98** (2018) no.5, 054025.
- [63] D. L. Yao, Masses and sigma terms of doubly charmed baryons up to $\mathcal{O}(p^4)$ in manifestly Lorentz-invariant baryon chiral perturbation theory, *Phys. Rev. D* **97** (2018) no.3, 034012.
- [64] M. Z. Liu, Y. Xiao and L. S. Geng, Magnetic moments of the spin-1/2 doubly charmed baryons in covariant baryon chiral perturbation theory, *Phys. Rev. D* **98** (2018) no.1, 014040.
- [65] Z. H. Guo, Prediction of exotic doubly charmed baryons within chiral effective field theory, *Phys. Rev. D* **96** (2017) no.7, 074004.
- [66] M. J. Yan, X. H. Liu, S. González-Solís, F. K. Guo, C. Hanhart, U. G. Meißner and B. S. Zou, New spectrum of negative-parity doubly charmed baryons: Possibility of two quasistable states, *Phys. Rev. D* **98** (2018) no.9, 091502.
- [67] L. Meng and S. L. Zhu, Light pseudoscalar meson and doubly charmed baryon scattering lengths with heavy diquark-antiquark symmetry, *Phys. Rev. D* **100** (2019) no.1, 014006.
- [68] P. C. Qiu and D. L. Yao, Chiral effective Lagrangian for doubly charmed baryons up to $\mathcal{O}(q^4)$, *Phys. Rev. D* **103** (2021) no.3, 034006.
- [69] Z. R. Liang and D. L. Yao, A unified formulation of one-loop tensor integrals for finite volume effects, *JHEP* **12** (2022), 029.
- [70] L. Liu, K. Orginos, F. K. Guo, C. Hanhart and U. G. Meissner, Interactions of charmed mesons with light pseudoscalar mesons from lattice QCD and implications on the nature of the $D_{s0}^*(2317)$, *Phys. Rev. D* **87** (2013) no.1, 014508.
- [71] M. Altenbuchinger, L. S. Geng and W. Weise, Scattering lengths of Nambu-Goldstone bosons off D mesons and dynamically generated heavy-light mesons, *Phys. Rev. D* **89** (2014) no.1, 014026.
- [72] D. L. Yao, M. L. Du, F. K. Guo and U. G. Meißner, One-loop analysis of the interactions between charmed mesons and Goldstone bosons, *JHEP* **11** (2015), 058.
- [73] M. L. Du, F. K. Guo, U. G. Meißner and D. L. Yao, Study of open-charm 0^+ states in unitarized chiral effective theory with one-loop potentials, *Eur. Phys. J. C* **77** (2017) no.11, 728.
- [74] M. Luscher, Volume Dependence of the Energy Spectrum in Massive Quantum Field Theories. 2. Scattering States, *Commun. Math. Phys.* **105** (1986), 153-188.
- [75] K. Rummukainen and S. A. Gottlieb, Resonance scattering phase shifts on a nonrest frame lattice, *Nucl. Phys. B* **450** (1995), 397-436.
- [76] C. h. Kim, C. T. Sachrajda and S. R. Sharpe, Finite-volume effects for two-hadron states in moving frames, *Nucl. Phys. B* **727** (2005), 218-243.
- [77] M. Gockeler, R. Horsley, M. Lage, U. G. Meissner, P. E. L. Rakow, A. Rusetsky, G. Schierholz and J. M. Zanotti, Scattering phases for meson and baryon resonances on general moving-frame lattices, *Phys. Rev. D* **86** (2012), 094513.
- [78] R. A. Briceno, Two-particle multichannel systems in a finite volume with arbitrary spin, *Phys. Rev. D* **89** (2014) no.7, 074507.
- [79] T. Becher and H. Leutwyler, Low energy analysis of $\pi N \rightarrow \pi N$, *JHEP* **06** (2001), 017.
- [80] G. F. Chew, M. L. Goldberger, F. E. Low and Y. Nambu, Application of Dispersion Relations to Low-Energy Meson-Nucleon Scattering, *Phys. Rev.* **106**, 1337-1344 (1957).

- [81] Goldberger, Marvin L and Watson, Kenneth M, Collision theory, Courier Corporation, 2004.
- [82] G. Höhler, Pion nucleon scattering. Part 2: Methods and results of phenomenological analyses, Landolt–Börnstein, 9, 1983.
- [83] W. R. Frazer and J. R. Fulco, Partial-Wave Dispersion Relations for Pion-Nucleon Scattering, Phys. Rev. **119** (1960), 1420-1426.
- [84] M. Hoferichter, J. Ruiz de Elvira, B. Kubis and U. G. Meißner, Roy–Steiner-equation analysis of pion–nucleon scattering, Phys. Rept. **625** (2016), 1-88.
- [85] J. A. Oller, M. Verbeni and J. Prades, Meson-baryon effective chiral lagrangians to $O(q^3)$, JHEP **09** (2006), 079.
- [86] A. Gomez Nicola and J. R. Pelaez, Meson meson scattering within one loop chiral perturbation theory and its unitarization, Phys. Rev. D **65** (2002), 054009.
- [87] R. L. Workman *et al.* [Particle Data Group], Review of Particle Physics, PTEP **2022** (2022), 083C01.
- [88] P. Di Vecchia and G. Veneziano, Chiral Dynamics in the Large n Limit, Nucl. Phys. B **171** (1980), 253-272.
- [89] R. Kaiser and H. Leutwyler, Large N_c in chiral perturbation theory, Eur. Phys. J. C **17** (2000), 623-649.
- [90] G. S. Bali *et al.* [RQCD], Masses and decay constants of the η and η' mesons from lattice QCD, JHEP **08** (2021), 137.
- [91] W. H. Press, S. A. Teukolsky, W. T. Vetterling and B. P. Flannery, Numerical Recipes in FORTRAN: The Art of Scientific Computing, ISBN: 9780521430647.
- [92] F. James, MINUIT Function Minimization and Error Analysis: Reference Manual Version 94.1, CERN-D-506.
- [93] J. Bijnens and G. Ecker, Mesonic low-energy constants, Ann. Rev. Nucl. Part. Sci. **64** (2014), 149-174.
- [94] G. Devaraj and R. G. Stuart, Reduction of one loop tensor form-factors to scalar integrals: A General scheme, Nucl. Phys. B **519** (1998), 483-513.
- [95] M. R. Schindler, D. Djukanovic, J. Gegelia and S. Scherer, Chiral expansion of the nucleon mass to order (q^*6) , Phys. Lett. B **649**, 390-393 (2007).
- [96] M. R. Schindler, D. Djukanovic, J. Gegelia and S. Scherer, Infrared renormalization of two-loop integrals and the chiral expansion of the nucleon mass, Nucl. Phys. A **803**, 68-114 (2008) [erratum: Nucl. Phys. A **1010**, 122175 (2021)].
- [97] M. Mai, P. C. Bruns, B. Kubis and U. G. Meissner, Aspects of meson-baryon scattering in three and two-flavor chiral perturbation theory, Phys. Rev. D **80** (2009), 094006.
- [98] J. X. Lu, L. S. Geng, X. L. Ren and M. L. Du, Meson-baryon scattering up to the next-to-next-to-leading order in covariant baryon chiral perturbation theory, Phys. Rev. D **99** (2019) no.5, 054024.
- [99] V. Crede and W. Roberts, Progress towards understanding baryon resonances, Rept. Prog. Phys. **76** (2013), 076301.
- [100] A. F. Falk, Hadrons of arbitrary spin in the heavy quark effective theory, Nucl. Phys. B **378** (1992), 79-94.

- [101] L. M. Nath, B. Etemadi and J. D. Kimel, Uniqueness of the interaction involving spin 3/2 particles, *Phys. Rev. D* **3** (1971), 2153-2161.
- [102] V. Pascalutsa and D. R. Phillips, Effective theory of the delta(1232) in Compton scattering off the nucleon, *Phys. Rev. C* **67**, 055202 (2003).
- [103] D. L. Yao, D. Siemens, V. Bernard, E. Epelbaum, A. M. Gasparyan, J. Gegelia, H. Krebs and U. G. Meißner, Pion-nucleon scattering in covariant baryon chiral perturbation theory with explicit Delta resonances, *JHEP* **05** (2016), 038.
- [104] Y. H. Chen, D. L. Yao and H. Q. Zheng, Analyses of pion-nucleon elastic scattering amplitudes up to $O(p^4)$ in extended-on-mass-shell subtraction scheme, *Phys. Rev. D* **87** (2013), 054019.
- [105] M. L. Du, F. K. Guo, U. G. Meißner and D. L. Yao, Aspects of the low-energy constants in the chiral Lagrangian for charmed mesons, *Phys. Rev. D* **94** (2016) no.9, 094037.
- [106] A. Denner and S. Dittmaier, Reduction schemes for one-loop tensor integrals, *Nucl. Phys. B* **734** (2006), 62-115.
- [107] J. Hu and T. Mehen, Chiral Lagrangian with heavy quark-diquark symmetry, *Phys. Rev. D* **73** (2006), 054003.
- [108] Z. W. Liu, Y. R. Liu, X. Liu and S. L. Zhu, The Pseudoscalar Meson and Heavy Vector Meson Scattering Lengths, *Phys. Rev. D* **84** (2011), 034002.
- [109] S. Z. Jiang, Y. R. Liu and Q. H. Yang, Chiral Lagrangians for mesons with a single heavy quark, *Phys. Rev. D* **99** (2019) no.7, 074018.